Title

Regulation of mitotic spindle disassembly by an environmental stress-sensing pathway in budding yeast.

Journal

Genetics, 198(3)

ISSN

0016-6731

Authors

Pigula, Adrianne
Drubin, David G
Barnes, Georjana

Publication Date

2014-11-01

DOI

10.1534/genetics.114.163238

Peer reviewed

Regulation of Mitotic Spindle Disassembly by an Environmental Stress-Sensing Pathway in Budding Yeast

Adrianne Pigula, David G. Drubin, and Georjana Barnes[1]
Department of Molecular and Cell Biology, University of California, Berkeley, California 94720

ABSTRACT Timely spindle disassembly is essential for coordination of mitotic exit with cytokinesis. In the budding yeast *Saccharomyces cerevisiae*, the microtubule-associated protein She1 functions in one of at least three parallel pathways that promote spindle disassembly. She1 phosphorylation by the Aurora kinase Ipl1 facilitates a role for She1 in late anaphase, when She1 contributes to microtubule depolymerization and shrinkage of spindle halves. By examining the genetic interactions of known spindle disassembly genes, we identified three genes in the environmental stress-sensing HOG (high-osmolarity glycerol response) pathway, *SHO1*, *PBS2*, and *HOG1*, and found they are necessary for proper localization of She1 to the anaphase spindle and for proper spindle disassembly. HOG pathway mutants exhibited spindle disassembly defects, as well as mislocalization of anillin-related proteins Boi1 and Boi2 from the bud neck. Moreover, Boi2, but not Boi1, plays a role in spindle disassembly that places Boi2 in a pathway with Sho1, Pbs2, and Hog1. Together, our data identify a process by which cells monitor events at the spindle and bud neck and describe a novel role for the HOG pathway in mitotic signaling.

MICROTUBULE dynamics play important roles in every stage of mitosis. In early M phase, interpolar microtubules help drive the separation of the spindle pole bodies (SPBs) to establish a bipolar spindle. As these interpolar microtubules (ipMTs) lengthen, the SPBs separate due to sliding forces generated by opposing microtubules originating from the opposite poles. In addition to ipMTs, kinetochore microtubules (kMTs) are attached to the kinetochore of each chromatid. A third class of microtubules, astral microtubules (aMTs), attach the SPBs to the cell cortex and help position the spindle along the mother-bud axis in yeast or perpendicular to the division plane in mammalian cells. Together, these three classes of MTs form the mitotic spindle. Over the course of mitosis, the dynamics of microtubules are modulated by several classes of proteins including +TIP proteins such as EB1/Bim1, which stabilize microtubule plus ends and promote growth, crosslinking proteins such as Ase1, which stabilize lateral interactions between ipMTs of the midzone, motor proteins such as Cin8 and Kip1, which generate forces necessary to slide the ipMTs by each other, and other motor proteins such as Kar3 and dynein (reviewed in Westermann *et al.* 2007; Khmelinskii and Schiebel 2008) that are also responsible for generating forces on MTs.

She1 is an important regulator of microtubule dynamics in budding yeast and it appears to have several functions in the cell (Woodruff *et al.* 2009, 2010; Bergman *et al.* 2012; Markus *et al.* 2012). Beginning in G1, She1 localizes to the SPB and restricts the activity of dynein by inhibiting its interaction with dynactin until anaphase, when dynein is required for spindle positioning prior to elongation into the bud (Woodruff *et al.* 2009). In M phase, She1 also localizes to the kinetochore and along spindle microtubules and to the bud neck (Woodruff *et al.* 2009, 2010). Upon completion of anaphase, She1 promotes spindle disassembly; *she1Δ* cells rely on contraction of the cytokinetic ring to induce spindle breakage, and spindle halves depolymerize at reduced rates in *she1Δ* cells (Woodruff *et al.* 2010).

Following chromosome biorientation and satisfaction of the spindle assembly checkpoint (SAC), several processes must coordinate anaphase and spindle disassembly. At a regulatory level, these include attenuating Cdk1 activity

doi: 10.1534/genetics.114.163238
Manuscript received August 1, 2014; accepted for publication August 28, 2014; published Early Online September 10, 2014.
Supporting information is available online at http://www.genetics.org/lookup/suppl/doi:10.1534/genetics.114.163238/-/DC1.
[1]Corresponding author: Department of Molecular and Cell Biology, University of California, Berkeley, 16 Barker Hall #3202, Berkeley, CA 94720-3202, Tel: (510) 642-5962. E-mail: gbarnes@berkeley.edu

by cyclin B destruction, and increasing the availability and activity of Cdc14 phosphatase via the FEAR and MEN pathways, to oppose Cdk1 activity and shift the cell into anaphase (Taylor *et al.* 1997; Visintin *et al.* 1998; reviewed in Stegmeier and Amon 2004; Sullivan and Morgan 2007). The mitotic kinase Ipl1, as part of the four subunit chromosomal passenger complex (CPC), also relocalizes to the spindle midzone at anaphase onset (Buvelot *et al.* 2003; Nakajima *et al.* 2011), where it participates in the NoCut pathway, a checkpoint that ensures that segregating chromosomes have cleared the midzone prior to cytokinetic ring contraction (Norden *et al.* 2006; Mendoza *et al.* 2009). The NoCut pathway monitors the presence of chromatin in the midzone via the activity of midzone-localized Ipl1 and communicates with cytokinesis machinery via the bud neck localization of the anillin-related proteins Boi1 and Boi2.

In contrast to spindle assembly, occurring from G1 through metaphase and spanning 30–40 min, spindle disassembly is rapid, occurring in <5 min at the end of anaphase (Maddox *et al.* 2000; Woodruff *et al.* 2010). At least three pathways contribute to spindle disassembly (Woodruff *et al.* 2010). One pathway involves the APC^{Cdh1}-dependent degradation of midzone proteins Cin8 and Ase1, which stabilize interpolar microtubules, leading to separation of the spindle halves. In a second pathway, the microtubule depolymerase Kip3 destabilizes microtubules and promotes shrinkage of spindle halves. A third pathway is dependent on the activity of Ipl1 toward spindle proteins. Phosphorylation of the microtubule stabilizing protein Bim1 by Ipl1 leads to Bim1 removal from the spindle and inhibits interpolar microtubule growth. Ipl1 phosphorylation of She1 on five residues is also important for its role in spindle disassembly. Mutating the five residues to phosphodefective alanines (*she1-5A*), or inhibiting Ipl1 function with a temperature-sensitive allele, leads to reduced She1 phosphorylation and delays in spindle disassembly in a manner similar to the *she1Δ* mutant (Woodruff *et al.* 2010). In this study, we further investigated the function of She1 by examining the contribution of the environmental stress-sensing HOG pathway and NoCut checkpoint proteins Boi1 and Boi2 to spindle disassembly.

Materials and Methods

Yeast strains and media

Yeast strains used in this study are listed in Supporting Information, Table S1. The *she1Δ*, *boi1Δ*, and *boi2Δ* strains originated in our lab and were generated by PCR product-mediated gene deletion (Longtine *et al.* 1998). The *sho1Δ* strain was from the Research Genetics collection and was backcrossed three times to DDY904 prior to use in experiments. The *pbs2Δ*, *hog1Δ*, and *hog1-as* strains were generously provided by the Thorner lab, and backcrossed three times to DDY904 prior to use. The *she1-2A* and *she1-2D* (T22A, T117A or T22D, T117D) mutants were generated using QuikChange site-directed mutagenesis (Stratagene) and incorporated at the endogenous *SHE1* locus. Yeast were maintained on YPD (yeast peptone medium with 2% glucose) using standard techniques.

Identifying candidate genes for spindle disassembly from genome-wide SGA studies

We identified mutants that were synthetic sick with *kip3Δ*, *cdh1Δ*, or *she1Δ* deletions by examining the supplemental data of Costanzo *et al.* (2010). We used the data set with an intermediate cutoff applied ($|\varepsilon| > 0.8$, P-value < 0.05). We identified those genes that shared genetic interactions with at least two of the three spindle disassembly genes (*kip3Δ*, *cdh1Δ*, and *she1Δ*), and chose to study candidates that, based on literature searches and additional large-scale analyses (mainly Tong *et al.* 2004; Tonikian *et al.* 2009), displayed genetic and/or physical interactions with mitotic or spindle disassembly genes.

Fluorescence microscopy

Starter cultures of cells to be imaged were grown overnight in minimal medium supplemented with 100 mM casamino acids (imaging medium). On the morning of the day of imaging, cells were diluted to 2.5×10^6 cells/ ml in imaging medium containing 10 mM *N*-acetyl-cysteine (to attenuate photobleaching). Cells were imaged at densities of 3.75–5 $\times$ 10^6 cells/ ml; capturing cells in early log phase was essential to properly detect She1–3GFP on the spindle and Boi1–GFP and Boi2–GFP at the bud neck.

Live cell microscopy at room temperature (23°) was performed using an IX-71 Olympus microscope with a 100× NA 1.4 objective and Orca-ER camera (Hamamatsu Photonics). For time-lapse microscopy of shrinking half spindles and cytokinetic ring contraction, images were collected at 10- and 30-sec intervals, respectively, with 300-msec exposures. For time-lapse microscopy of She1–3GFP, images were collected at 1-min intervals, with 300-msec exposures. Each image represents a maximum intensity projection from a z stack containing five planes 0.4 μm apart. For still images of Boi1–GFP and Boi2–GFP, z stacks of seven images spaced 0.4 μm apart were collected to encompass the entire plasma membrane and were acquired using 700-msec exposures. Dual-color imaging of Cdc14–GFP or She1–3GFP and mCherry–Tub1 was performed with an IX-81 Olympus microscope equipped with a temperature-controlled enclosure (Precision Control Weather Station), a 100× NA 1.4 objective, and an Orca-ER camera. Images were obtained by sequential switching between RFP and GFP filter sets. All image processing was performed using MetaMorph and ImageJ.

For experiments with the *hog1-as* allele, 30 μM 1NM–PP1 in DMSO (or an equal volume of DMSO) was added to cultures 3 hr prior to imaging and was maintained in this medium at the same concentration while the cells were imaged. For *cdc15-2* experiments, cells were shifted to 37° for

1 hr prior to imaging at 23°; the temperature-sensitive phenotype of this allele is readily reversible, so that within 10–15 min of release from 37° arrest, cells were exiting mitosis and Cdc14 release could be imaged coincident with spindle breakdown.

TCA precipitation and immunoblots

For the phospho-Hog1 blots, cells were grown in YPD to ~6.25×10^6 cells/ml prior to sorbitol addition. Sorbitol, 3 M, in YPD was added to a final sorbitol concentration of 1 M and cultures were rapidly mixed and incubated for 5 min. For the nocodazole time course, Hog1–GFP cells were grown to a density of ~6.25×10^6 cells/ml, and 10 μg/ ml nocodazole (in DMSO) was added for 3 hr. Nocodazole was washed out with medium containing 1% DMSO (cell pellets were washed twice with YPD containing 1% DMSO and once with YPD without DMSO). Cells, ~1.25×10^7, were harvested at each time point; cells were spun down and rapidly washed with 20% TCA (Sigma Aldrich) to destroy protease activity and maintain phosphorylation, and pellets were snap frozen in liquid nitrogen and stored at −80°. To lyse cells, pellets were thawed on ice and 250 μl 20% TCA was added, in addition to ~200 μl 0.5-mm acid-washed glass beads (Sigma Aldrich). Samples were vortexed on the highest setting for 10 min at 4°, and then a 22-G needle was heated and used to poke a hole in the bottom of the Eppendorf tube, and the tube was inserted into a second Eppendorf tube and centrifuged at 2000 rpm for 3 min in a microfuge at 4°. Glass beads were washed with 350 μl 5% TCA, centrifuged at 2000 rpm for 3 min in a microfuge at 4°, and the flow-through was combined with an additional 750 μl 5% TCA. The TCA precipitate was briefly vortexed and pelleted at 14,000 rpm for 10 min in a microfuge at 4°. The pellet was washed with 1 ml 100% ice-cold ethanol and then air dried and resuspended in 1 M Tris pH 8.0 and SDS loading buffer such that there were ~1.25×10^5 cells/μl. For phospho-Hog1 blots, 10 μl of sample was loaded per lane on a 10% SDS–PAGE gel, transferred to nitrocellulose membranes, and probed with 1:1000 rabbit α-phospho-p38 antibodies (clone D3F9, Cell Signaling Technology), 1:1000 rabbit α-GFP antibodies (Torrey Pines Biolabs), 1:500 rabbit α-Clb2 antibodies (Santa Cruz Biotechnology), and 1:1000 mouse α-Pgk1 antibodies (Molecular Probes). For She1–myc blots, 5 μl of sample was loaded per lane on an 8% SDS–PAGE gel supplemented with 24 μM Phos-Tag acrylamide (Wako Chemicals USA) and 24 μM $MnCl_2$. Phos-Tag gels were run at a constant amperage of 10 mA, transferred to nitrocellulose membranes, and probed with either 1:1000 mouse α-Myc antibodies (clone 9E10, purified by the Drubin/Barnes lab) or 1:1000 mouse α-Pgk1 (Molecular Probes). 1:10,000 IRDye 800 or IRDye 680 secondary antibodies (Li-Cor Biosciences) were used to detect bands on a Li-Cor Odyssey (Li-Cor Biosciences). ImageJ was used to quantify band intensities; levels of phospho-Hog1 and total Hog1-GFP were first normalized by Pgk1 levels, and then the level of phospho-Hog/total Hog1-GFP was calculated. Time courses with hydroxyurea arrested cells were similarly performed, except hydroxyurea was added to cultures at a final concentration of 0.2 M, and cells were washed twice with YPD to release the arrest.

Results

The environmental stress-sensing HOG pathway has genetic and physical interactions with spindle disassembly pathways

We examined genome-wide synthetic genetic array (SGA) interaction data (Costanzo *et al.* 2010) in an effort to identify additional candidate genes participating in the She1 spindle disassembly pathway. This approach was successfully used in the past to identify novel components of spindle disassembly pathways (Woodruff *et al.* 2010). We applied the logic that if there are three spindle disassembly pathways, represented by *KIP3*, *CDH1*, and *SHE1*, compromising the function of any two of these pathways would cause a synthetic growth defect. For example, if a gene deletion produces a growth defect in combination with the *kip3Δ* mutant, the gene would hypothetically function in either the *CDH1* or *SHE1* spindle disassembly pathways. If the same deletion produces a growth defect in combination with the *cdh1Δ* mutant, the candidate gene would be presumed to function in the *SHE1* pathway. We therefore searched specifically for gene deletion strains possessing negative genetic interaction scores with both *kip3Δ* and *cdh1Δ* (Figure 1A). Interestingly, a deletion mutant of *SHO1*, which encodes an osmosensor, showed negative genetic interactions with both *kip3Δ* and *cdh1Δ* mutants.

Sho1 is a transmembrane protein component of the HOG pathway that acts as a sensor of osmotic (sorbitol) stress (Brewster *et al.* 1993; Maeda *et al.* 1995; Posas and Saito 1997; Raitt *et al.* 2000; Reiser *et al.* 2006; Cullen *et al.* 2004; reviewed in Schwartz and Madhani 2004; Clotet and Posas 2007). Cells exposed to 1 M sorbitol initiate a Sho1-dependent MAPK (mitogen-activated protein kinase) signaling cascade that requires the scaffold Ste11, Msb2, and the MAPKK Pbs2. Pbs2 phosphorylation activates the MAPK Hog1, which transiently translocates into the nucleus to stimulate transcription of genes involved in glycerol production.

HOG pathway activation has also been implicated in early cell-cycle arrest due to Hog1's transcriptional downregulation of *CLN1* and *CLN2*, which encode G1 cyclins, and phosphorylation of the DNA synthesis inhibitor Sic1, which stabilizes it against degradation and therefore slows S phase (Escoté *et al.* 2004). Moreover, Hog1 activation also inhibits cyclin–Cdk1 activity, which delays G2 (Alexander *et al.* 2001). HOG pathway activation has also been shown to promote mitotic exit (Reiser *et al.* 2006). Shocking cells osmotically with medium containing sorbitol rescues the anaphase arrest of *cdc15-2* mutants in a *SHO1*-dependent manner. This rescue has been linked to the Pbs2-dependent

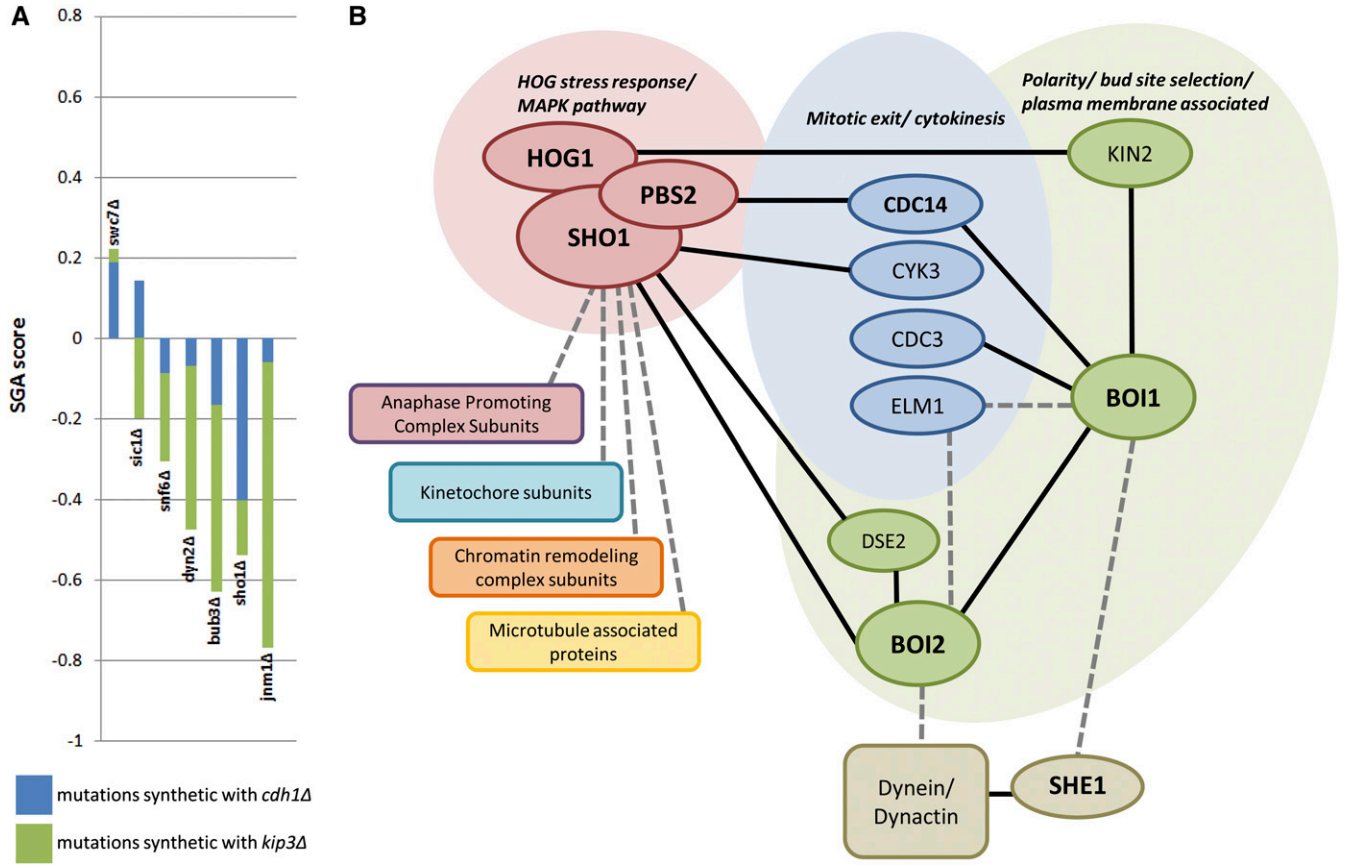

Figure 1 The transmembrane osmosensor Sho1 and the associated HOG pathway are candidates for regulating spindle disassembly. (A) Comparison of synthetic genetic array (SGA) scores for genes that showed synthetic interactions with *kip3Δ* and *cdh1Δ* deletion mutants. For each gene represented by a bar on the graph, the SGA scores between that gene and *kip3Δ* (in green) and *cdh1Δ* (in blue) are represented by the magnitude of the bar in the graph. Negative values represent negative genetic interactions (the double mutant cells grew worse than either single mutant cell), and positive values represent positive genetic interactions (the double mutant cells grew better than either single mutant cells). (B) Schematic of genetic interactions (dashed lines) and physical interactions (solid lines) between genes/proteins involved in the HOG pathway (top left), kinetochore and spindle organization (bottom left), cytokinetic ring organization and function (middle), and polarity pathways (right). Interactions were described using annotations curated by the SGD database (http://www.yeastgenome.org).

release of Cdc14 phosphatase from the nucleolus (Reiser *et al.* 2006).

We further examined the genetic and physical interaction profiles of HOG pathway components (Figure 1B). We noted that in high-throughput, genome-wide screens (Tong *et al.* 2004; Costanzo *et al.* 2010), the *sho1Δ* mutant showed multiple genetic interactions with mitotic genes including those encoding microtubule-associated proteins, APC subunits in addition to Cdh1, kinetochore subunits, and chromatin remodeling complexes. While these genetic interactions appeared specific to Sho1, and not to the HOG pathway in general, other components of the HOG pathway exhibit physical interactions with proteins in cell polarity pathways, and with bud neck-localized proteins that have been implicated in cytokinesis (Tong *et al.* 2004; Costanzo *et al.* 2010). Sho1 itself localizes to the cell cortex of emerging bud tips and growing buds and to the bud neck during cytokinesis (Raitt *et al.* 2000). Interestingly, the NoCut pathway proteins Boi1 and Boi2 show similar localization patterns, as well as genetic interactions with dynein subunits (Tong *et al.* 2004; Norden *et al.* 2006; Costanzo *et al.* 2010). Additionally, Boi2 physically interacts with Sho1 (Drees *et al.* 2001; Tong *et al.* 2002).

HOG pathway mutants and boi2Δ mutant cells exhibit spindle disassembly defects

We investigated whether *sho1Δ*, *pbs2Δ*, and *hog1Δ* mutants show any spindle disassembly defects. We used a Myo1–GFP fusion protein to mark the cytokinetic ring and a GFP–Tub1 protein to identify the mitotic spindle. We used these two fluorescent proteins in conjunction to determine when the spindle separated into halves relative to the time when the cytokinetic ring began to constrict (Figure 2). As previously described, wild-type spindles broke to form two half spindles before the cytokinetic ring began to constrict (Figure 2A, left; Woodruff *et al.* 2010). This sequence of events can be seen in a kymograph showing GFP–Myo1 fluorescence over time (Figure 2A, right). However, similar to *she1Δ* spindles, *sho1Δ*, *pbs2Δ*, and *hog1Δ* spindles broke into half spindles only after the cytokinetic ring began to constrict (Figure

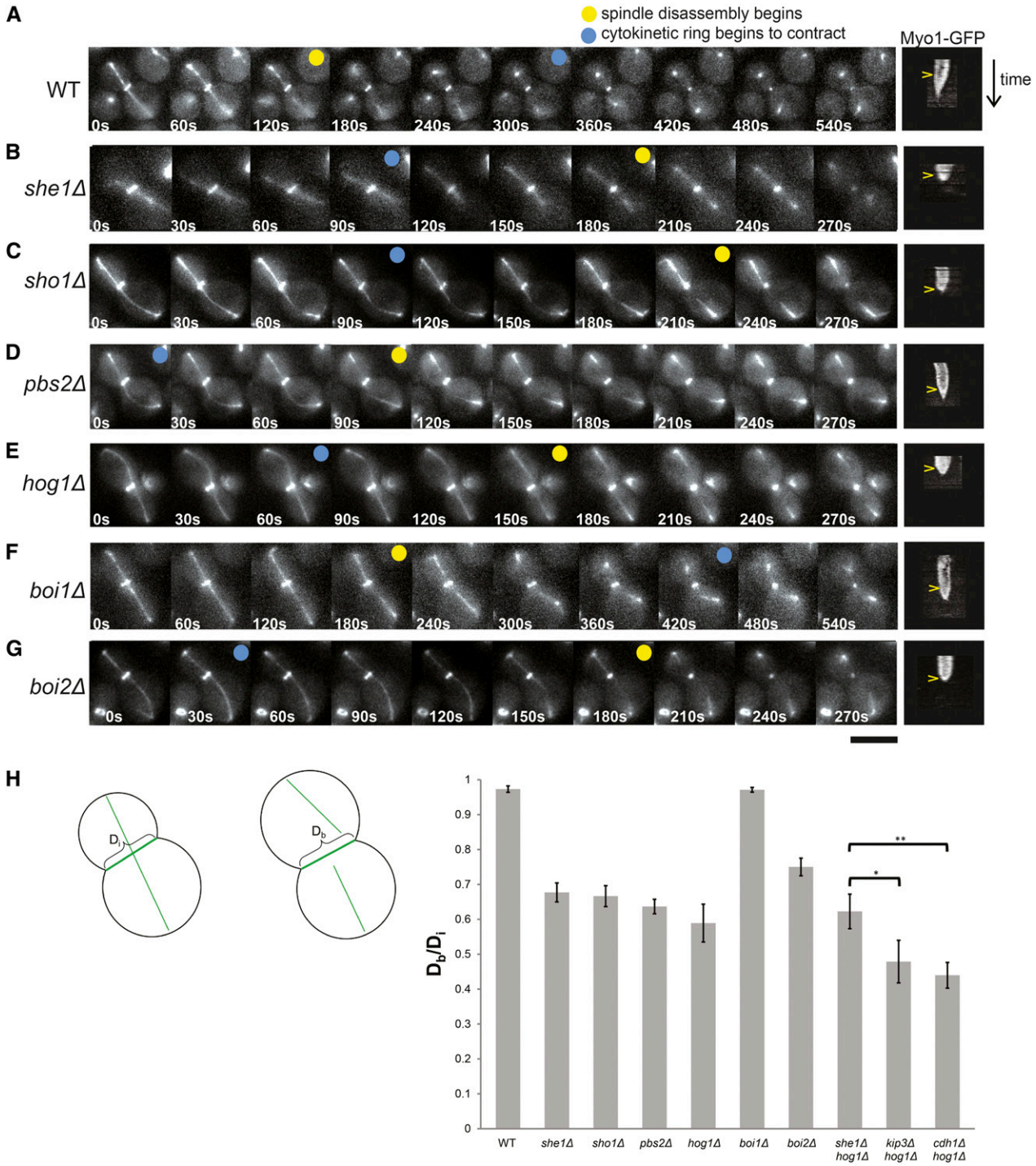

Figure 2 Cytokinetic ring contraction precedes spindle disassembly in HOG pathway mutants and *boi2*Δ cells. (A–G) Left: time-lapse images of indicated strains possessing integrated *GFP–TUB1* and *MYO1–GFP* markers, to label the spindle and bud neck, respectively. Images were captured 30 sec apart at 23°, but have been selected to show similar events for each strain. Right: kymograph showing the cytokinetic ring over time (time proceeds from top to bottom; pixels in the kymographs are 30 sec apart). Yellow arrowheads indicate when the spindle breaks. Bar, 5 μm. (H) Initial length of Myo1–GFP fluorescence was measured when the bud neck was the widest (D_i) and when the spindle broke (D_b). D_b/D_i ratios were plotted (error bars represent SEM)

2, B–E). We quantified this phenotype by measuring the diameter of the cytokinetic ring at its maximum size, before the spindles had broken (Figure 2H, initial diameter, D_i). We also measured the diameter of the cytokinetic ring when the spindle broke into half spindles (diameter at break, D_b), and compared D_b/D_i ratios. The wild-type D_b/D_i ratio was 0.97 ±0.01 (Figure 2H), reflecting the observation that the cytokinetic ring had not begun to constrict when the spindle

broke. However, D_b/D_i ratios for *she1Δ*, *sho1Δ*, *pbs2Δ*, and *hog1Δ* mutants were 0.68 (±0.03), 0.67 (±0.03), 0.64 (±0.02), and 0.59 (±0.02), respectively. These results indicate that the cytokinetic ring has constricted 30–40% by the time the spindles break in these cells.

Because of the many genetic and physical interactions between the HOG pathway, Boi1 and Boi2, and She1, we wanted to determine if *boi1Δ* and *boi2Δ* mutants showed spindle disassembly defects. Strikingly, *boi2Δ* spindles showed a delay in spindle disassembly similar to HOG pathway and *she1Δ* mutants; the D_b/D_i ratio for *boi2Δ* cells was 0.75 ±0.03 (Figure 2, G and H). However, we determined that *boi1Δ* spindle disassembly appeared indistinguishable from wild type, as *boi1Δ* spindles disassembled before ring contraction, and the D_b/D_i ratio for *boi1Δ* cells was 0.97 ±0.01 (Figure 2, F and H).

Additionally, we analyzed the timing of cytokinetic ring contraction relative to spindle disassembly in three double mutants, *she1Δ hog1Δ*, *kip3Δ hog1Δ*, *cdh1Δ hog1Δ* mutants (Figure 2H). We found that spindles in all three mutants broke after the cytokinetic ring began to contract; the D_b/D_i ratio for the *she1Δ hog1Δ* double mutant was 0.62 ±0.05 and not significantly different than either the *she1Δ* or *hog1Δ* single mutant. However, both the *kip3Δ hog1Δ* double mutant and the *cdh1Δ hog1Δ* double mutant had D_b/D_i ratios that were significantly reduced compared to the *she1Δ hog1Δ* double mutant (0.48 ±0.06 for *kip3Δhog1Δ* and 0.44 ±0.04 for *cdh1Δhog1Δ*). The additive effect of the *HOG1* deletion with either *KIP3* or *CDH1* deletion on spindle disassembly corroborates that *HOG1* is likely in a different spindle disassembly pathway than *KIP3* or *CDH1*. Relatedly, the fact that the *she1Δ hog1Δ* double mutant did not have a more severe phenotype than either the *she1Δ* or *hog1Δ* mutants suggests that *SHE1* and *HOG1* are in the same pathway of spindle disassembly.

We also studied the kinetics with which mitotic half spindles depolymerized in these HOG pathway mutants and *boi1Δ* and *boi2Δ* mutants. Previous work used analysis of microtubule depolymerization rates and the frequency of microtubule rescue events to help define three spindle disassembly pathways present in wild-type cells that together are essential for viability (Woodruff *et al.* 2010). We noted that prior to spindle breakage, the spindles of cells with a *sho1Δ*, *pbs2Δ*, *hog1Δ*, or *boi2Δ* mutation often bowed and bent severely (Figure 3, C–E and G). When the spindles broke, they often broke in the interior of the mother or daughter cell rather than in the wild-type location of the site of cytokinesis. It is possible that a weak "stress point" was introduced where the spindle bowed and bending at that location resulted in spindle breakage. This phenotype was similar to that seen for *she1Δ* spindles, but was distinct from spindle breakage for wild-type and *boi1Δ* cells, wherein the spindles remained straight and broke near the site of cytokinesis (Figure 3, A, B, and F).

Half-spindle depolymerization rates also reflected a similarity between the *she1Δ* mutant and *sho1Δ*, *pbs2Δ*, *hog1Δ*, and *boi2Δ* mutant cells (Table 1). All of these mutants showed reduced spindle disassembly rates, which were on the same order as the *she1Δ* mutant, consistent with the conclusion that these genes function in the same pathway. As another example of the functional difference between *boi1Δ* and *boi2Δ* mutants, *boi1Δ* half-spindle shrinkage rates were indistinguishable from those in wild-type cells. These results suggest distinct functions for Boi1 and Boi2. We could not evaluate spindle phenotypes of *boi1Δ boi2Δ* spindles because the double mutant is inviable in our strain background.

Our spindle disassembly data, particularly the reduced spindle–half shrinkage rates, suggest that mitotic exit is slowed in HOG pathway mutants and *she1Δ* and *boi2Δ* cells. However, it is possible that cytokinesis may be accelerated in these mutants, and spindles break prematurely as the cytokinetic ring constricts. To address this possibility, we used Mtw1–GFP, a kinetochore marker, in conjunction with Myo1–GFP. We measured the time between sister kinetochore separation in early to mid-mitosis, which is marked by a single Mtw1–GFP signal splitting into two foci as chromosomes segregate, and the initiation of cytokinetic ring contraction, as observed by the shrinking of Myo1–GFP signal (Figure S1A). We found that the cytokinetic ring began to contract ~33 min after Mtw1–GFP foci separation in wild-type cells, and ~45 min after Mtw1–GFP foci separation in *she1Δ* and *hog1Δ* mutants (Figure S1B). We conclude that *she1Δ* and *hog1Δ* mutants spend a longer time in mitosis, likely owing to difficulties in spindle disassembly, rather than undergoing accelerated cytokinesis, which prematurely breaks spindles into spindle halves.

Boi1 and Boi2 are mislocalized from the bud neck in HOG pathway mutants

We used a genomically integrated GFP tag fused to either Boi1 or Boi2 to observe the localization of these proteins in HOG pathway mutants. In *sho1Δ*, *pbs2Δ*, and *hog1Δ* cells, we observed a polarized distribution for Boi1 and Boi2 (Norden *et al.* 2006; Figure S2A). As previously reported, Boi1 and Boi2 localized to the cortex of daughter cells as buds emerged in S phase and continued growing during G2. However, in large budded cells (late M phase), all of the detectable Boi1 and Boi2 relocalized to the bud neck in ~55% of wild-type cells (Figure 4). Additionally, a smaller but significant portion of large budded wild-type cells did not display Boi1 or Boi2 at the bud neck or elsewhere near the cortex; in ~40% of cells for Boi1–GFP, and 30% of cells for Boi2–GFP, the GFP fusion proteins could not be detected anywhere in the cell. However, in *sho1Δ*, *pbs2Δ*, and *hog1Δ* cells, we found that both Boi1 and Boi2 were mislocalized from the bud neck of large-budded cells. In *sho1Δ* cells, Boi1 was entirely displaced from the bud neck and was randomly distributed in puncta throughout the mother cell and bud (Figure 4A, yellow arrows). Boi2 only partially localized to the bud neck in *sho1Δ* cells, although it appeared to be recruited to the cell cortex near the bud neck more so than

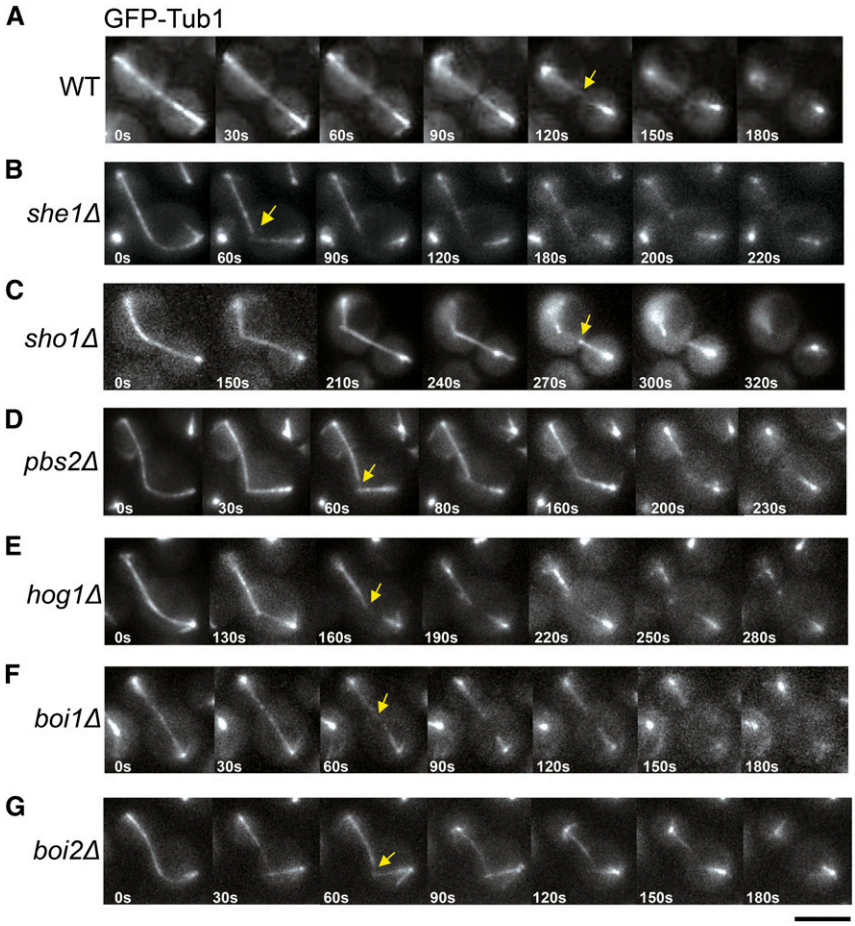

Figure 3 Spindle disassembly is delayed in HOG pathway and *boi2*Δ mutants. (A–G) Time-lapse images of strains expressing GFP–Tub1 to monitor spindle disassembly. Images were captured 10 sec apart at 23°, but have been selected to show similar events for each strain. Yellow arrows indicate when the spindle breaks. Bar, 5 μm.

Boi1. In *pbs2Δ* and *hog1Δ* cells, Boi1 and Boi2 were able to localize to the bud neck similar to wild-type cells only <20% of the time. Most often, these cells displayed additional patches of Boi1 and Boi2 elsewhere on the cell cortex. These patches often occurred on the cortex adjacent to the bud neck, although they were also found elsewhere along the cortex (Figure 4A). Neither Boi1 nor Boi2 was mislocalized from the bud neck in *she1Δ* cells. Boi1 and Boi2 localization in cells of each genotype was quantified (Figure 4B).

Sho1 is a transmembrane protein, which localizes to the bud neck (Raitt *et al.* 2000). Therefore, Boi1 and Boi2 mislocalization could be an indirect consequence of upsetting the structural integrity of the bud neck. To evaluate whether this was the case, we checked the localization of the septin Cdc3, which localizes as a ring at the bud neck (Madden and Snyder 1998), in HOG pathway mutants. In *sho1Δ*, *pbs2Δ*, and *hog1Δ* mutant cells, Cdc3–GFP localized to the bud neck in a wild-type manner (Figure S2B), even in cells that appeared to have multiple bud necks as a result of failed cell divisions. This result suggests that Boi1 and Boi2 mislocalization in HOG pathway mutants is specific and is not a consequence of general bud neck disorganization. It is also not a consequence of altered Boi1–GFP or Boi2–GFP expression in HOG pathway mutants, since protein levels were approximately equal between all the mutants examined (Figure S2C).

She1 is mislocalized in HOG pathway mutants and boi2Δ mutants

Because the delay in spindle disassembly for HOG pathway and *boi2Δ* mutants was evocative of a *she1Δ* spindle disassembly phenotype, we evaluated She1 protein localization in *sho1Δ*, *pbs2Δ*, *hog1Δ*, and *boi2Δ* mutants. In wild-type cells, She1–3GFP localizes to the SPBs and decorates short, metaphase spindles very brightly. As the spindle begins to elongate in anaphase, however, She1 is cleared from the midzone, and becomes enriched near the spindle poles (Figure 5A). She1 also localizes to the bud neck throughout mitosis until the end of anaphase. However, because the She1 population at the bud neck is obscured by She1 fluorescence at the spindle, it is difficult to determine whether bud neck intensity changes over the course of mitosis and precisely when it disappears from the bud neck.

When we examined She1–3GFP in *sho1Δ* cells, we found that it still localized to SPBs, the spindle, and the bud neck (Figure 5B). However, it was not cleared from the midzone as in wild-type cells. Instead, She1–3GFP decorated the entire spindle brightly throughout anaphase in 90% of anaphase *sho1Δ* cells. Strikingly, in these *sho1Δ* cells, She1 often remained associated with the plus ends of depolymerizing microtubules once the spindle broke into spindle

Table 1 Half-spindle depolymerization rates are decreased in hog pathway and *boi2Δ* mutants

	Half-spindle shrinkage rate (μm/sec)	Recovery frequency (F_{rec}/sec)	*n*	*P*-value
WT	0.064 (±0.003)	0.006	116	N/A
she1Δ	0.037 (±0.003)	0.006	110	<0.001
sho1Δ	0.034 (±0.002)	0.006	117	<0.001
pbs2Δ	0.035 (±0.003)	0.014	233	<0.001
hog1Δ	0.033 (±0.004)	0.006	102	<0.001
boi1Δ	0.061 (±0.005)	0.005	50	0.53
boi2Δ	0.037 (±0.002)	0.006	125	<0.001
hog1-as no drug/no DMSO	0.061 (±0.004)	0.008	139	N/A*
hog1-as +DMSO	0.060 (±0.003)	0.007	188	0.94*
hog1-as +1NM–PP1	0.040 (±0.003)	0.008	155	<0.001*
she1-2A	0.039 (±0.003)	0.006	132	<0.001
she1-2D hog1Δ	0.060 (±0.004)	0.008	48	0.32
she1-2D hog1-as no drug/no DMSO	0.060 (±0.004)	0.005	37	N/A**
she1-2D hog1-as +DMSO	0.060 (±0.005)	0.006	17	0.87**
she1-2D hog1-as +1NM-PP1	0.060 (±0.003)	0.007	54	0.79**

GFP–Tub1-expressing strains were imaged every 10 sec, and lengths of half spindles were measured at each time point after the spindles broke. Recovery events were scored each time a half spindle switched from shrinking to growing. Shrinkage rates were calculated from the slope of the half-spindle lengths when plotted *vs.* time and reported as mean (±SEM). *P*-values were determined by a model I analysis of variance test when the wild-type shrinkage rate was directly compared to the rates of mutants. *, strains that were compared to the *hog1-as* no drug/no DMSO control. **, strains that were compared to the *she1-2D hog1-as* no drug/no DMSO control.

halves, a localization pattern never observed in wild-type cells. To ensure that we were observing She1 localization along the spindle in *sho1Δ* cells and other mutants, we performed dual-color, live-cell imaging of She1–3GFP and mCherry–Tub1 to mark the spindle (Figure S3A). We do not prefer to use strains with *mCherry–TUB1* because in our hands this version of *TUB1*, unlike *GFP–TUB1*, appears to have a synthetic growth defect with deletions or tagged versions of other spindle-related genes. We did, however, find that She1–3GFP colocalized with mCherry–Tub1 in all of the mutants we examined. We also found that She1–3GFP expression was not elevated or altered in any of the mutants we observed (Figure S3B).

In *pbs2Δ*, *hog1Δ*, and *boi2Δ* mutant cells, similar to *sho1Δ* cells, She1 inappropriately localized along the length of the spindle as it elongated (Figure 5, C, D, and F, and Figure S3A). However, She1–3GFP did not appear to decorate the entire spindle as densely or as thoroughly in *pbs2Δ*, *hog1Δ*, and *boi2Δ* mutants, compared to *sho1Δ* cells. This contrasted with *boi1Δ* mutant cells, wherein She1 localization appeared as in wild-type cells, further highlighting a difference between *boi1Δ* and *boi2Δ* mutations.

We noted that She1 localization is dependent in part on cell density. In the experiments we presented, we were careful to image only cells that were in the early part of log phase. In mid-log phase (3.75–5 × 10^6 cells/ml), She1–3GFP does not localize to the spindle as well, but appears as diffuse staining throughout the cell, although it does localize to the bud neck. Similarly, Boi1–GFP and Boi2–GFP tend to have a hazy and diffuse appearance within the cytoplasm if cells are too dense (data not shown). This phenomenon is not only important to take into consideration when studying the localization of these proteins, but is interesting in that it implies that the functions of these proteins are coupled to aspects of cell physiology associated with cell density and potentially with cell growth and polarity pathways.

Hog1 kinase activity is required for spindle disassembly

The HOG pathway stimulates phosphorylation of the MAP kinase Hog1 in response to sorbitol stress. Because we hypothesized that the HOG pathway affects spindle disassembly through She1, we were interested in exploring the relationship between She1, Hog1, and mitotic exit. We used the sensitized background of a *cdc15-2* mutant, a temperature-sensitive allele of the mitotic exit network kinase Cdc15. Growing *cdc15-2* cells on medium containing sorbitol rescues the temperature sensitivity of the allele in a HOG pathway-dependent manner (Reiser *et al.* 2006; Figure S4A). We found that, like *HOG1* and *PBS2*, *SHE1* contributed to the rescue of the *cdc15-2* mutant on sorbitol plates (Figure S4A) although less robustly than HOG pathway genes. We also treated asynchronously growing cells with sorbitol and examined She1 phosphorylation (Figure S4B). She1–myc was rapidly phosphorylated within 2 min of sorbitol treatment (see arrow at right in Figure S4B, and note the initial decrease in nonphosphorylated She1–myc). These growth and phosphorylation data corroborate the idea that She1 is associated with the HOG pathway, both in response to osmotic stress and during mitotic exit.

We were interested in determining if She1 is a Hog1 kinase substrate. We first assessed whether Hog1 is phosphorylated and activated in a cell-cycle-dependent manner. We synchronized cells in metaphase with nocodazole and used a phospho-specific Hog1 antibody to detect Hog1 phosphorylation at time points after nocodazole washout (Figure 6, A and B). Levels of phospho-Hog1 were elevated in the first 30 min after nocodazole release. Hog1 phosphorylation decreased ~45 min after nocodazole release, coincident with the degradation of cyclin B, indicating anaphase onset. We also observed elevated levels of phospho-Hog1 in cells released from a hydroxyurea arrest; in these cells, phospho-Hog1 levels also decreased as cyclin B levels decreased

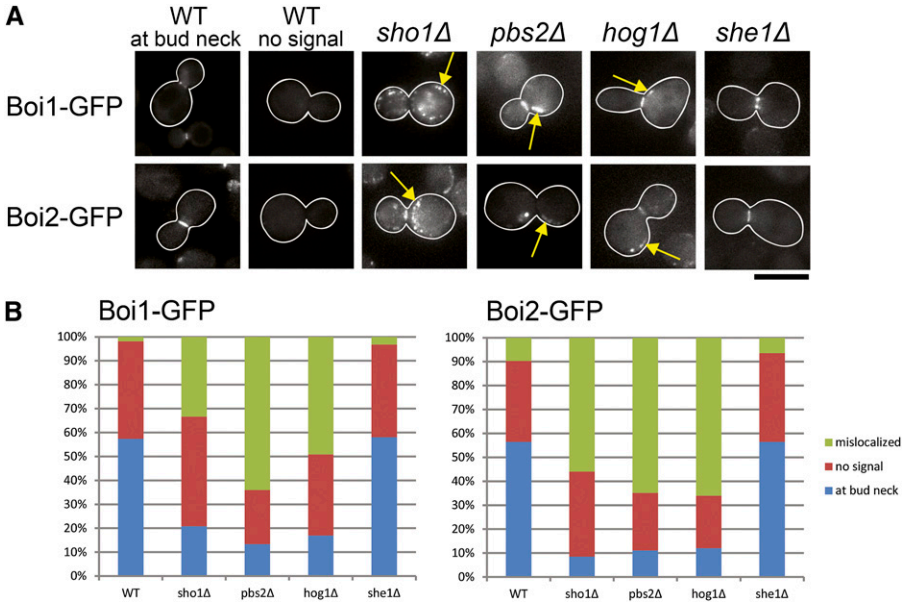

Figure 4 Boi1 and Boi2 are mislocalized in HOG pathway mutants. (A) Epifluorescent images of live large-budded cells with the indicated genotype and carrying endogenously tagged Boi1–GFP (top) or Boi2–GFP (bottom). Yellow arrows indicate patches of Boi1 or Boi2 that are mislocalized from the bud neck. Bar, 5 μm. (B) Quantitation of Boi1 and Boi2 mislocalization. Approximately 130 large-budded cells from 3 different days were scored for each strain. "At bud neck" indicates Boi1 or Boi2 localized properly to the bud neck; "no signal" indicates that no Boi1 or Boi2 was present at the bud neck or plasma membrane; "mislocalized" indicates that Boi1 or Boi2 localized either away from the bud neck or to other regions of the cell in addition to the bud neck.

(Figure S4C, 75- and 90-min timepoints). These data indicate that Hog1 is active in a cell-cycle-dependent manner and is active at a relevant time in mitosis to affect spindle dynamics.

We analyzed the sequence of *Saccharomyces cerevisiae* She1 for putative Hog1 consensus sites, based on the motif identified in Mok *et al.* (2010). We found two residues in She1, Thr22 and Thr117, which fit the phosphorylation consensus site of Hog1. We mutated these residues to alanines at the endogenous *SHE1* locus to create a *she1-2A* allele, which displayed poor growth compared to wild-type or *she1-Δ* cells (Figure S4D). We evaluated the phosphorylation of She1-2A–13myc by PhosTag gel electrophoresis and immunoblot (Figure 6C). She1-2A appeared less phosphorylated than wild-type She1, as evidenced by a decrease in the ladder of bands, indicating that Thr22 and Thr117 are phosphorylated *in vivo*. However, this decrease in phosphorylated She1-2A was not due to a difference in expression levels between She1-2A–myc and She1-WT–myc (Figure S4E)

We also evaluated the spindle disassembly phenotype of the *she1-2A* allele, as well as an analog-sensitive allele of Hog1 (Westfall and Thorner 2006), *hog1-as* (Figure 6, D and E). In wild-type cells, spindles broke ~2.43 (±0.17) min *before* the Myo1–GFP signal disappeared at the end of cytokinetic ring contraction. In *hog1Δ* mutant cells, although spindle disassembly is delayed until after the cytokinetic ring begins to contract, the Myo1–GFP signal typically does not entirely disappear before the spindles break (however, in 6/39 instances, the Myo1–GFP signal disappeared before the spindle broke, Figure 6E). Spindles in *hog1Δ* mutant cells broke ~2.03 (±0.28) min before the Myo1–GFP signal disappeared; the spindle disassembly delay of this mutant is reflected in the ~0.4-min shift in the timing of spindle breakage, relative to wild-type cells. However, *she1-2A* cells showed dramatic delays in spindle breakage; in this mutant, spindles bent in a manner reminiscent of HOG pathway mutants and *boi2Δ* cells and broke ~3.48 (±0.22) min *after* the disappearance of Myo1–GFP signal. This is nearly a 6-min delay in spindle breakage compared to wild-type cells. Once spindles of *she1-2A* cells broke, they showed delays in depolymerization that were similar to HOG pathway mutants and *boi2Δ* cells (Table 1).

A small delay in spindle breakage was observed in control *hog1-as* cells not treated with drug or carrier DMSO (−1.13 ±0.20 min), or treated with DMSO alone (0.42 ±0.23 min). We interpret these findings as an indication that the *hog1-as* allele may not be fully functional, at least in regard to the spindle disassembly function of Hog1. Analog-sensitive alleles do have mutations in their ATP-binding pockets, and it is possible that the Hog1-as kinase may not bind ATP as well as Hog1. It also appears that the addition of DMSO compounds this problem slightly. However, the half-spindle shrinkage rates for *hog1-as* cells not treated with drug or DMSO, or treated with DMSO alone, were comparable to wild-type shrinkage rates (Table 1).

When we treated *hog1-as* cells with the inhibitor 1NM–PP1, we saw a dramatic delay in spindle disassembly, of the same magnitude as that of *she1-2A* mutant cells. Spindles broke ~3.48 (±0.22) min after the Myo1–GFP signal disappeared, and half spindles depolymerized more slowly, with a rate similar to that of *she1Δ*, *boi2Δ*, and HOG pathway mutants (Figure 6, D and E and Table 1).

We next determined whether She1 localization along the spindle is perturbed in the *she1-2A* and *hog1-as* mutants. The *she1-2A* allele grows poorly, and *she1-2A–3GFP* mutants were too sick to allow reliable evaluation of She1 localization (data not shown). However, in *hog1-as* cells treated with 1NM–PP1, She1–3GFP foci localized along the spindle as the spindle elongated, in a manner similar to what we observed in the *boi2Δ* mutant and HOG pathway mutants

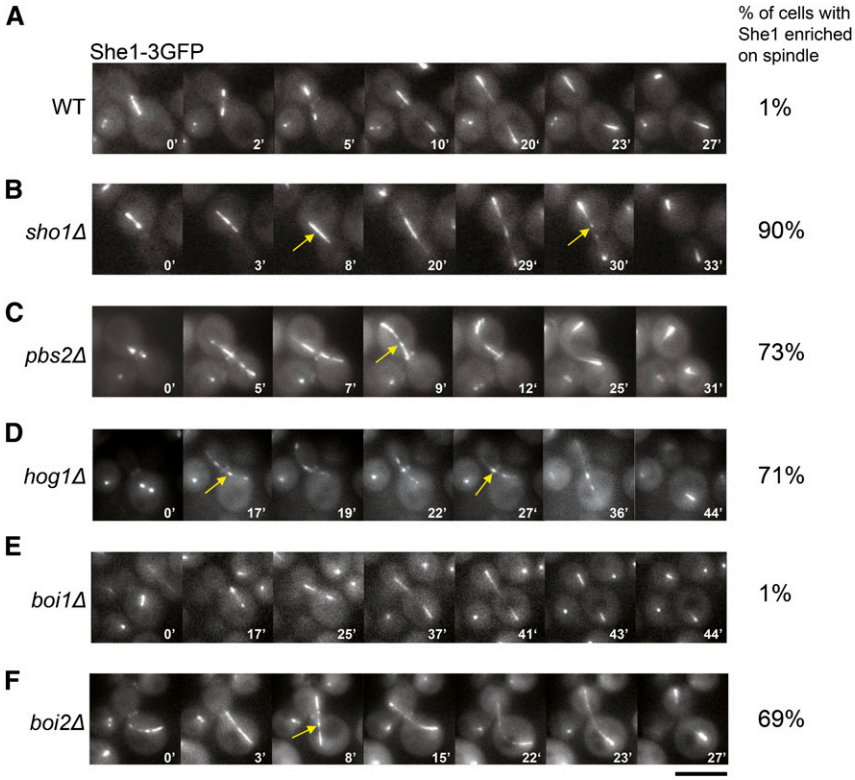

Figure 5 She1 is mislocalized along the spindle in HOG pathway mutants and *boi2*Δ cells. (A–F) Time-lapse images of endogenously tagged She1–3GFP strains of the indicated genotype. She1 is present at the bud neck in all strains. Whereas in wild-type cells, She1 is cleared from the spindle midzone as the spindle elongates, and HOG pathway mutants and *boi2Δ* cells retain She1 at the spindle midzone (yellow arrows). Approximately 50 cells of each genotype were scored for She1 enrichment on the spindle. Bar, 5 μm.

(Figure 6F). Together, these data indicate that Hog1 kinase activity affects clearance of She1 from the spindle, the timely initiation of spindle breakage, and effective half-spindle depolymerization.

We also created a phosphomimetic allele of *SHE1*, *she1-2D*, wherein we exchanged the putative Hog1 phosphorylated residues for aspartates. This allele grew better than the *she1-2A* allele (Figure S4C) and was able to suppress the spindle disassembly phenotype of *hog1Δ* cells. The spindles of *she1-2D hog1Δ* cells broke before the cytokinetic ring began to contract, and ~2.51 (±0.24) min before the Myo1–GFP signal disappeared, indistinguishable from wild-type cells (Figure 6, D and E). Spindles of *she1-2D hog1Δ* cells were also straight and broke near the bud neck, similar to wild-type cells and in contrast to HOG pathway mutants and *she1Δ* mutant cells. Interestingly, the *she1-2D* allele also rescued the *hog1-as* spindle phenotype. Even when untreated, or treated with DMSO, the spindles of *she1-2D hog1-as* cells broke well before the Myo1–GFP signal disappeared (Figure 6, D and E). There was still a slight effect from the addition of DMSO, but our results for these conditions trend toward wild-type results, and when we added the inhibitor 1NM–PP1 to *she1-2D hog1-as* cells, spindles broke ~2.19 (±0.22) min before Myo1–GFP disappearance. As with the *she1-2D hog1Δ* double mutant, spindles of *she1-2D hog1-as* cells were straight and broke near the bud neck, and half spindles depolymerized with wild-type kinetics (Figure 6D and Table 1).

Our data illustrate that Thr22 and Thr117 are important residues in She1, and because we saw deleterious effects from the *she1-2A* allele, and rescue of the *hog1* loss of function phenotypes with the *she1-2D* allele, we strongly suspect that Thr22 and Thr117 are regulated by Hog1 phosphorylation *in vivo*. We have endeavored to examine She1 phosphorylation *in vivo*, using a number of techniques. At this time it is difficult to make definitive conclusions about the contribution of Hog1 to She1 phosphorylation, because She1 is also highly phosphorylated by Ipl1. However, when we synchronized cells with hydroxyurea, and collected cells in a time-course fashion after washout, we were able to detect some changes in She1 phosphorylation in *hog1Δ* cells (Figure S4F). One phosphorylated species in particular seems to be reduced in *hog1Δ* cells (Figure S4F, see arrow).

Cdc14 localization is perturbed in she1Δ and hog1Δ cells

PBS2 is required for mitotic exit in a *cdc15-2* mutant exposed to sorbitol stress, and this escape from a *cdc15-2* arrest is dependent on Cdc14 release from the mother cell nucleolus (Reiser *et al.* 2006). In agreement with Reiser *et al.* (2006), we found that the *pbs2Δ* mutant, as well as *hog1Δ* and *she1-Δ* mutants, did not show marked delays in Cdc14 release from the mother cell nucleolus in nonstress conditions. However, we did find that once released from the nucleolus, Cdc14 does not reincorporate into mother and daughter cell nucleoli in a timely fashion (Figure 7A). We used a *cdc15-2 CDC14–GFP mCherry–TUB1* strain to evaluate Cdc14 localization in nonstress conditions. The *cdc15-2* allele was used to arrest cells in anaphase, and cultures were shifted to 23° to evaluate Cdc14 localization in nonstress conditions as cells escaped arrest and exited mitosis. In wild-type cells,

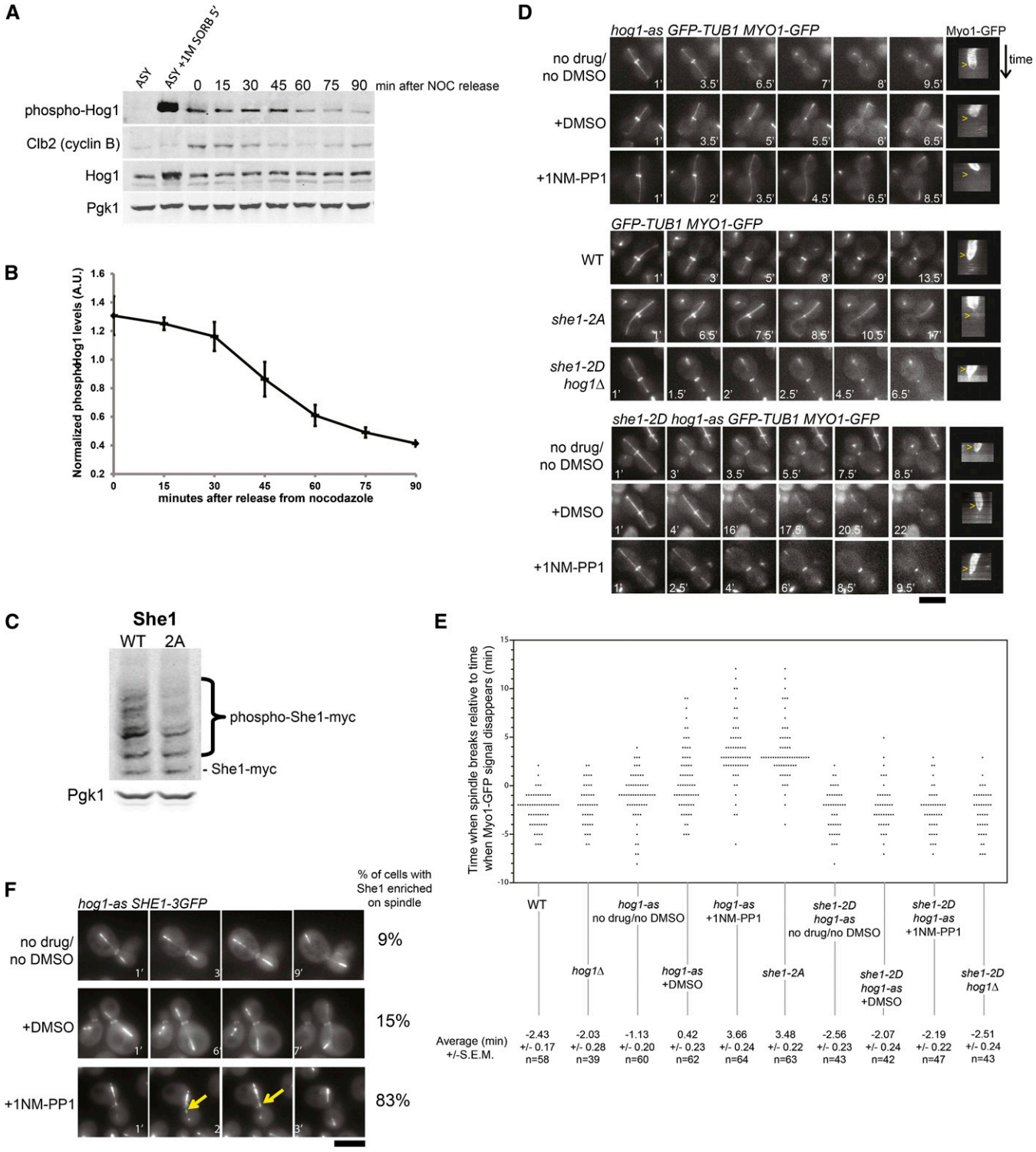

Figure 6 Hog1 kinase activity is required for spindle disassembly and She1 spindle localization. (A) Hog1 is phosphorylated in a cell-cycle-dependent manner. Immunoblots of TCA-precipitated whole-cell extracts from Hog1–GFP-expressing cells were probed with antibodies against phosphorylated Hog1, GFP (total Hog1), and Clb2. Cells were collected every 15 min after nocodazole (NOC) arrest and washout. ASY: asynchronously growing cultures that were not stressed, or stressed for 5 min with 1 M sorbitol to induce Hog1 phosphorylation. (B) Quantification of Hog1 phosphorylation during mitotic exit. Levels of phospho-Hog1 were normalized against total Hog1 levels and Pgk1 levels and plotted over time. Three separate experiments were analyzed; error bars represent SEM. (C) The She1-2A mutant is less phosphorylated than She1–WT. Immunoblot of TCA-precipitated whole-cell extracts run on a Phos-Tag gel and probed with anti-myc antibodies. (D) Spindle disassembly in the *hog1-as* mutant (top) and *she1-2A* mutant (top middle) is delayed until after cytokinetic ring contraction. A phosphomimetic *she1-2D* allele rescues *hog1Δ* spindle disassembly defects (bottom middle), and *hog1-as* spindle disassembly defects (bottom). Left: time-lapse images of indicated strains possessing integrated *GFP–TUB1* and *MYO1–GFP* markers

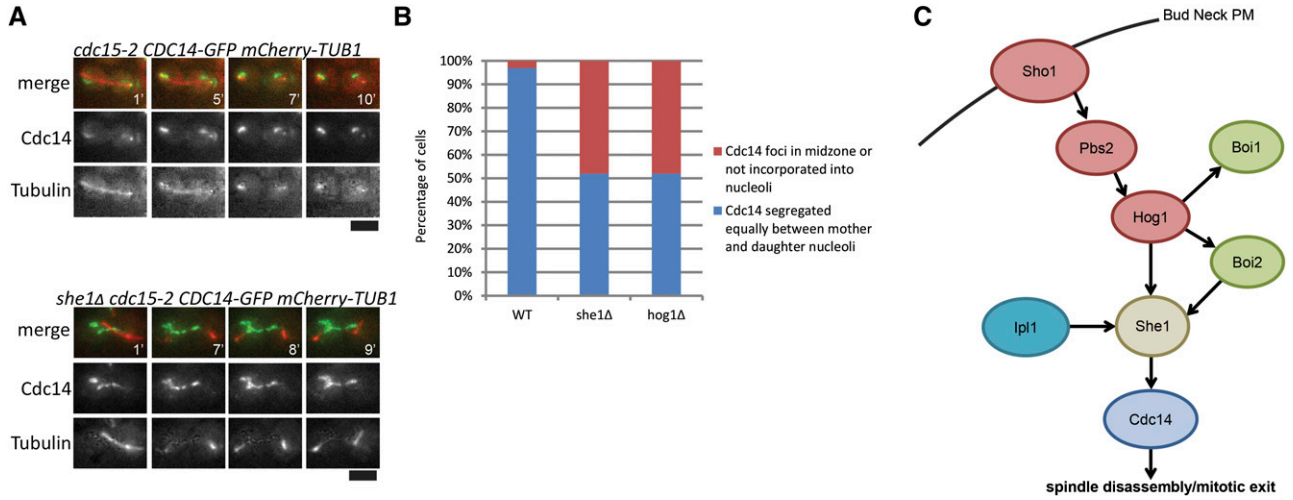

Figure 7 Cdc14 is mislocalized in *she1Δ* and *hog1Δ* mutants. (A) Time-lapse images of wild-type (top) and *she1Δ* (bottom) strains expressing Cdc14–GFP and mCherry–Tub1. The *cdc15-2* allele was used to synchronize cells by inducing anaphase arrest at 37° for 1 hr prior to imaging at 23°. Bar, 5 μm. (B) Quantification of the Cdc14 mislocalization phenotype. Approximately 100 cells were scored for each strain. (C) Model for the effect of the HOG pathway on She1 function and spindle disassembly.

Cdc14 was resequestered equally between mother and daughter cell nucleoli before the spindle broke an half spindles depolymerized. In *pbs2*Δ, *hog1*Δ, and *she1*Δ mutant cells, Cdc14 did not segregate evenly between mother and daughter cells, but became stuck in the spindle midzone and was not efficiently recruited into nucleoli in ~50% of cells (Figure 7B).

Discussion

For several years it has been known that She1 localizes to the mitotic spindle, bud neck, spindle pole bodies, and astral MTs (Wong *et al.* 2007, 2009, 2010). Previous work described She1's role in inhibiting dynein activity until it is required for spindle positioning in anaphase (Woodruff *et al.* 2009) and showed that She1 phosphorylation by Ipl1 is required to promote spindle disassembly (Woodruff *et al.* 2010). In this study, we expanded our knowledge of the She1 spindle disassembly pathway by investigating the contribution of the HOG pathway and NoCut checkpoint proteins Boi1 and Boi2 to the regulation of She1 localization and spindle disassembly. Based on the results of our experiments, we have constructed a model for how the HOG pathway influences spindle disassembly through She1 (Figure 7C).

The HOG pathway contributes to spindle disassembly through She1 function

We found the HOG pathway mutants *sho1Δ*, *pbs2Δ*, and *hog1Δ* exhibit spindle disassembly phenotypes similar to the *she1Δ* mutant; they do not disassemble spindles until after cytokinetic ring contraction begins, and once spindles have broken into half spindles, microtubules depolymerize ~1.7× slower than in wild-type cells. She1 localization is also perturbed in HOG pathway mutants. Although She1 still localizes to the bud neck in *sho1Δ*, *pbs2Δ*, and *hog1Δ* cells, it strongly decorates the spindle at inappropriate times during anaphase, as if it cannot be excluded or removed from the spindle midzone. This finding highlights the somewhat paradoxical nature of She1: although She1 binds and diffuses along microtubules *in vitro* (Markus *et al.* 2012) and is required for timely spindle disassembly in wild-type cells (Woodruff *et al.* 2010; this study), it does not strongly localize to the site most critical to the destabilization of spindle microtubules during anaphase, the midzone. Moreover, She1 localization in the HOG pathway mutants and *boi2Δ* cells shows that enriching She1 at the midzone, or in the case of the *sho1Δ* mutant even at the depolymerizing ends of spindle microtubules, does not promote spindle disassembly.

These results indicate that there is a complexity to She1 function and regulation that we do not yet understand. In wild-type cells and in every deletion mutant we studied, She1 was eventually removed from the bud neck during anaphase. The cell may use She1 localization as a way of signaling between the spindle and bud neck, similar to the manner in which the NoCut pathway coordinates chromosome segregation with cytokinesis. At the bud neck, the HOG pathway may promote interactions between She1

(time proceeds from top to bottom; pixels in the kymographs are 30 sec apart). Yellow arrowheads indicate when the spindle breaks. Bar, 5 μm. (E) Quantification of spindle disassembly delays. Time (in minutes) was measured between the disappearance of Myo1–GFP signal and when the spindle broke. Negative values indicate that the spindle broke before the cytokinetic ring contracted and Myo1–GFP signal disappeared, while positive values indicate that the spindle broke after the Myo1–GFP disappeared. (F) Time-lapse images of endogenously tagged She1–3GFP in the *hog1-as* background. Yellow arrows indicate She1 mislocalized along the spindle. Approximately 60 cells were scored for each condition. Bar, 5 μm.

and other proteins that are necessary for She1 signaling. These interactions or post-translational modifications may be disrupted in HOG pathway mutants, such that She1 loses a feature necessary for its role in spindle disassembly. Hence, although more She1 localizes to the spindle in HOG pathway mutants and *boi2Δ* cells, it is not competent to promote spindle disassembly.

We observed that in ~50% of *pbs2Δ*, *hog1Δ*, and *she1Δ* mutants, although Cdc14 was released from the mother cell nucleolus in a timely fashion, it was not resequestered into mother and bud nucleoli by the time the spindle had disassembled, a behavior we rarely observed in wild-type cells. It is difficult to infer mechanisms from this phenotype, however, because the phenotype may be a consequence of either the delays in spindle disassembly exhibited by these mutants or perturbed signaling at the bud neck. In our model we propose that the effects on Cdc14 localization are downstream of the HOG pathway and She1, but we acknowledge that Cdc14 may be an upstream regulator of She1 that, for example, dephosphorylates She1 or helps exclude She1 from the bud neck in late anaphase. Unfortunately designing an experiment to address these questions is made challenging by the facts that *cdc14* temperature-sensitive alleles arrest prior to spindle disassembly and that Cdc14-specific inhibitors are not available.

Distinct functions for the anillin-related proteins Boi1 and Boi2

Prior studies led to the conclusion that Boi1 and Boi2 functions are redundant paralogs based on their localization patterns, genetic and physical interactions, regulation, and structural homology: both proteins contain Ipl1 and Cdk1 phosphorylation consensus sites, N-terminal SH3 domains, and C-terminal pleckstrin homology (PH) domains (Norden *et al.* 2006; Mendoza *et al.* 2009). Here we have shown that while Boi1 and Boi2 are mislocalized from the bud neck in HOG pathway mutants, She1 is mislocalized in *boi2*Δ, but not in *boi1*Δ, mutants. Furthermore, only the *boi2*Δ mutant has a spindle disassembly phenotype that mimics that of a *she1*Δ mutant. These data suggest that the HOG pathway functions through Boi2 to promote She1-dependent spindle disassembly.

The significance of the Boi1 and Boi2 mislocalization patterns is not clear. Localization differed slightly between *sho1*Δ cells and *pbs2*Δ or *hog1*Δ cells. In the *sho1*Δ mutant, we noted that most of the Boi1 and Boi2 was not at the bud neck, but was cortically associated, whereas in *pbs2Δ* and *hog1Δ* mutants, at least some of the Boi1 and Boi2 localized to the bud neck. This observation implicates Sho1 in recruitment of Boi1 and Boi2 to the cortex or plasma membrane, a possibility that could be further tested by direct tests for Sho1 interaction with Boi1 and Boi2.

Norden *et al.* (2006) proposed that when at the bud neck, Boi1 and Boi2 delay cytokinesis through the NoCut pathway by inhibiting the activity of septins and that when Boi1 and Boi2 are removed from the bud neck, cytokinesis proceeds. However, despite moderate (in the case of *pbs2Δ* and *hog1Δ* mutants) to severe (in the case of the *sho1Δ* mutant) displacement of Boi1 and Boi2 from the bud neck, we did not observe premature cytokinesis in any of these mutants. We did note that a small percentage (~5%) of *pbs2Δ* and *hog1Δ* cells appeared multibudded and had two spindles, perhaps reflecting a defect in the NoCut pathway during previous cell divisions. Coupled with the data showing a spindle disassembly delay for the *boi2Δ* mutant, the localization data for Boi1 and Boi2 suggest that these proteins are not only involved in the inhibition of septin function, but are involved in monitoring other aspects of mitotic exit as well. Interesting findings by the Kellogg lab support the idea that Boi1 is regulated by Cdk1 phosphorylation and is a component of a pathway whereby Cdk1 monitors the overall growth and polarity of the cell (McCusker *et al.* 2007; Anastasia *et al.* 2012). It is unclear what impact, if any, Ipl1 phosphorylation has on Boi1 and Boi2; although Ipl1 activity is essential to the NoCut pathway, phosphomutants of Boi1 and Boi2 are not mislocalized (Norden *et al.* 2006). It is now important to determine whether Boi2 is regulated more by Ipl1 than Cdk1 phosphorylation and whether it is a component of the pathway whereby Ipl1 monitors spindle integrity and chromosome segregation. Our findings that place Boi2, but not Boi1, in a pathway with She1 and spindle disassembly support a model wherein Boi1 and Boi2 are monitoring slightly different aspects of cell division (cell growth for Boi1 and nuclear division for Boi2) and wherein signaling from both Boi1 and Boi2 is integrated at the bud neck to promote timely cytokinesis.

The role of She1 phosphorylation

She1 is phosphorylated by Ipl1, and this phosphorylation is important for She1's role in spindle disassembly (Woodruff *et al.* 2010). In this study we found that Hog1 kinase is phosphorylated and activated in a cell-cycle-dependent manner and that abolishing Hog1 kinase activity by using a *hog1-as* allele produces spindle disassembly phenotypes and She1 mislocalization phenotypes that are similar to phenotypes of HOG pathway mutants and *she1Δ* and *boi2Δ* mutants. Furthermore, a *she1-2A* allele that is phosphodefective at Hog1 consensus sites is not efficiently phosphorylated *in vivo* and also shows delays in spindle disassembly, which can be rescued by a phosphomimetic version of She1. These data suggest that She1 may be directly phosphorylated by Hog1 kinase. In the future it will be important to dissect the regulation of She1 by Ipl1 and Hog1 kinases. It is possible that these two kinases regulate different aspects of She1 function or that one kinase catalyzes priming phosphorylations on She1, to increase the availability or affinity of She1 as a substrate for the other kinase and that full phosphorylation by both kinases is important for She1 function.

HOG pathway activity during mitosis

We began this project by investigating the contribution of Sho1 to spindle disassembly and we decided to analyze

spindle disassembly phenotypes in the absence of osmotic stress, since this was the condition used in the screen that first identified genetic interactions between *sho1*Δ and *cdh1*Δ and *kip3*Δ (Costanzo *et al.* 2010). We also thought it important to understand whether the *sho1*Δ mutant, and later, other HOG pathway mutants, had functions apart from their signaling roles in osmotically stressed cells. Our results show that Hog1 is phosphorylated and activated during mitosis and that the HOG pathway has a role in spindle disassembly even under unstressed conditions, but also raise the question of how the HOG pathway, which depends on hierarchical activation of kinases Pbs2 and Hog1 via a MAPK signaling cascade, accomplishes its effects in the absence of a stress signal. The mechanism by which Sho1 responds to osmotic stress is still unclear, other than that it depends in part on an accessory transmembrane protein, Msb2 (Cullen *et al.* 2004). One possibility is that during mitosis the structure or curvature of the plasma membrane at the bud neck changes, inducing a conformational change in Sho1 and/or Msb2 that results in transient activation of the HOG pathway during mitotic exit. Alternatively, since Msb2 is a putative substrate of Cdk1 (Ubersax *et al.* 2003), and since both Sho1 and Msb2 interact with the Cdc42 pathway (Raitt *et al.* 2000), which influences septin organization and the actomyosin cytokinetic ring, there may be mitotic inputs into the HOG pathway in the form of phosphoregulation or mitotic-specific protein–protein interactions that induce activation.

Acknowledgments

The authors thank Jeff Woodruff, Anthony Cormier, Jeremy Thorner, Jesse Patterson, Yuko Nakajima, and Randall Tyers for helpful discussion and the lab of Jeremy Thorner for *pbs2Δ*, *hog1Δ*, and *hog1-as* strains and the Cdc3-GFP plasmid. This work was supported by National Institutes of Health GM 47842 to G.B.

Literature Cited

Alexander, M. R., M. Tyers, M. Perret, B. M. Craig, K. S. Fang *et al.*, 2001 Regulation of cell cycle progression by Swe1p and Hog1p following hypertonic stress. Mol. Biol. Cell 12: 53–62.

Anastasia, S. D., D. L. Nguyen, V. Thai, M. Meloy, T. MacDonough *et al.*, 2012 A link between mitotic entry and membrane growth suggests a novel model for cell size control. J. Cell Biol. 197: 89–104.

Bergman, Z. J., X. Xia, I. A. Amaro, and T. C. Huffaker, 2012 Constitutive dynein activity in She1 mutants reveals differences in microtubule attachment at the yeast spindle pole body. Mol. Biol. Cell 23: 2319–2326.

Buvelot, S., S. Y. Tatsutani, D. Vermaak, and S. Biggins, 2003 The budding yeast Ipl1/Aurora protein kinase regulates mitotic spindle disassembly. J. Cell Biol. 160: 329–339.

Brewster, J. L., T. de Valoir, N. D. Dwyer, E. Winter, and M. C. Gustin, 1993 An osmosensing signal transduction pathway in yeast. Science 259: 1760–1763.

Clotet, J., and F. Posas, 2007 Control of cell cycle in response to osmostress: lessons from yeast. Methods Enyzomol. 428: 63–76.

Costanzo, M., A. Baryshnikova, J. Bellay, Y. Kim, E. D. Spear *et al.*, 2010 The genetic landscape of a cell. Science 327: 425–431.

Cullen, P. J., W. Sabbagh, Jr., E. Graham, M. M. Irick, E. van Olden *et al.*, 2004 A signaling mucin at the head of the Cdc42- and MAPK-dependent filamentous growth pathway in yeast. Genes Dev. 18: 1695–1708.

Drees, B. L., B. Sundin, E. Brazeau, J. P. Caviston, G. C. Chen *et al.*, 2001 A protein interaction map for cell polarity development. J. Cell Biol. 154: 549–571.

Escoté, X., M. Zapater, J. Clotet, and F. Posas, 2004 Hog1 mediates cell-cycle arrest in G1 phase by the dual targeting of Sic1. Nat. Cell Biol. 2004: 997–1002.

Khmelinskii, A., and E. Schiebel, 2008 Assembling the spindle midzone in the right place at the right time. Cell Cycle 7: 283–286.

Longtine, M. S., A. McKenzie, 3rd, D. J. Demarini, N. G. Shah, A. Wach *et al.*, 1998 Additional modules for versatile and economical PCR-based gene deletion and modification in *Saccharomyces cerevisiae*. Yeast 14: 953–961.

Madden, K., and M. Snyder, 1998 Cell polarity and morphogenesis in budding yeast. Annu. Rev. Microbiol. 52: 687–744.

Maddox, P. S., K. S. Bloom, and E. D. Salmon, 2000 The polarity and dynamics of microtubule assembly in the budding yeast *Saccharomyces cerevisiae*. Nat. Cell Biol. 2: 36–41.

Maeda, T., M. Takekawa, and H. Saito, 1995 Activation of yeast PBS2 MAPKK by MAPKKKs or by binding of an SH3-containing osmosensor. Science 269: 554–558.

Markus, S. M., K. A. Kalutkiewicz, and W. L. Lee, 2012 She1-mediated inhibition of dynein motility along astral microtubules promotes polarized spindle movements. Curr. Biol. 22: 1–10.

McCusker, D., C. Denison, S. Anderson, T. A. Egelhofer, J. R. Yates, 3rd, *et al.*, 2007 Cdk1 coordinates cell-surface growth with the cell cycle. Nat. Cell Biol. 9: 506–515.

Mendoza, M., C. Norden, K. Durrer, H. Rauter, F. Uhlmann *et al.*, 2009 A mechanism for chromosome segregation sensing by the NoCut checkpoint. Nat. Cell Biol. 11: 477–483.

Mok, J., P. M. Kim, H. Y. Lam, S. Piccirillo, X. Zhow *et al.*, 2010 Deciphering protein kinase specificity through large-scale analysis of yeast phosphorylation site motifs. Sci. Signal. 109: ra12.

Nakajima, Y., A. Cormier, R. G. Tyers, A. Pigula, Y. Peng *et al.*, 2011 Ipl1/Aurora-dependent phosphorylation of Sli15/INCENP regulates CPC-spindle interaction to ensure proper microtubule dynamics. J. Cell Biol. 194: 137–153.

Norden, C., M. Mendoza, J. Dobbelaere, C. V. Kotwaliwale, S. Biggins *et al.*, 2006 The NoCut pathway links completion of cytokinesis to spindle midzone function to prevent chromosome breakage. Cell 125: 85–98.

Posas, F., and H. Saito, 1997 Osmotic activation of the HOG MAPK pathway via Ste11p MAPKKK: scaffold role of Pbs2p MAPKK. Science 276: 1702–1705.

Raitt, D. C., and F. Posas, and H. Saito, 2000 Yeast Cdc42 GTPase and Ste20 PAK-like kinase regulate Sho1-dependent activation of the Hog1 MAPK pathway. EMBO J. 19: 4623–4631.

Reiser, V., K. E. D'Aquino, L. S. Ee, and A. Amon, 2006 The stress-activated mitogen-activated protein kinase signaling cascade promotes exit from mitosis. Mol. Biol. Cell 17: 3136–3146.

Schwartz, M. A., and H. D. Madhani, 2004 Principles of MAP kinase signaling specificity in *Saccharomyces cerevisiae*. Annu. Rev. Genet. 38: 725–748.

Stegmeier, F., and A. Amon, 2004 Closing mitosis: the functions of the Cdc14 phosphatase and its regulation. Annu. Rev. Genet. 38: 203–232.

Sullivan, M., and D. O. Morgan, 2007 Finishing mitosis, one step at a time. Nat. Rev. Mol. Cell Biol. 8: 894–903.

Taylor, G. S., Y. Liu, C. Baskerville, and H. Charbonneau, 1997 The activity of Cdc14p, an oligomeric dual specificity

protein phosphatase from *Saccharomyces cerevisiae*, is required for cell cycle progression. J. Biol. Chem. 272: 24054–24063.

Tong, A. H., B. Drees, G. Nardelli, G. D. Bader, B. Brannetti *et al.*, 2002 A combined experimental and computational strategy to define protein interaction networks for peptide recognition modules. Science 295: 321–324.

Tong, A. H., G. Lesage, G. D. Bader, H. Ding, H. Xu *et al.*, 2004 Global mapping of the yeast genetic interaction network. Science 303: 808–813.

Tonikian, R., X. Xin, C. P. Toret, D. Gfeller, C. Landgraf *et al.*, 2009 Bayesian modeling of the yeast SH3 domain interactome predicts spatiotemporal dynamics of endocytosis proteins. PLoS Biol. 7: e1000218.

Ubersax, J. A., E. L. Woodbury, P. N. Quang, M. Paraz, J. D. Blethrow *et al.*, 2003 Targets of the cyclin-dependent kinase Cdk1. Nature 425: 859–864.

Visintin, R., K. Craig, E. S. Hwang, S. Prinz, M. Tyers *et al.*, 1998 The phosphatase Cdc14 triggers mitotic exit by reversal of Cdk-dependent dephosphorylation. Mol. Cell 2: 709–718.

Westermann, S., D. G. Drubin, and G. Barnes, 2007 Structure and functions of yeast kinetochore complexes. Annu. Rev. Biochem. 76: 563–591.

Westfall, P. J., and J. Thorner, 2006 Analysis of mitogen-activated protein kinase signaling specificity in response to hyperosmotic stress: use of an analog-sensitive HOG1 allele. Eukaryot. Cell 5: 1215–1228.

Wong, J., Y. Nakajima, S. Westermann, C. Shang, J. S. Kang *et al.*, 2007 A protein interaction map of the mitotic spindle. Mol. Biol. Cell 10: 3800–3809.

Woodruff, J. B., D. G. Drubin, and G. Barnes, 2009 Dynein-driven mitotic spindle positioning restricted to anaphase by She1p inhibition of dynactin recruitment. Mol. Biol. Cell 20: 3003–3011.

Woodruff, J. B., D. G. Drubin, and G. Barnes, 2010 Mitotic spindle disassembly occurs via distinct subprocesses driven by the anaphase-promoting complex, Aurora B kinase, and kinesin-8. J. Cell Biol. 191: 795–808.

Communicating editor: M. D. Rose

GENETICS

Supporting Information
http://www.genetics.org/lookup/suppl/doi:10.1534/genetics.114.163238/-/DC1

Regulation of Mitotic Spindle Disassembly by an Environmental Stress-Sensing Pathway in Budding Yeast

Adrianne Pigula, David G. Drubin, and Georjana Barnes

DOI: 10.1534/genetics.114.163238

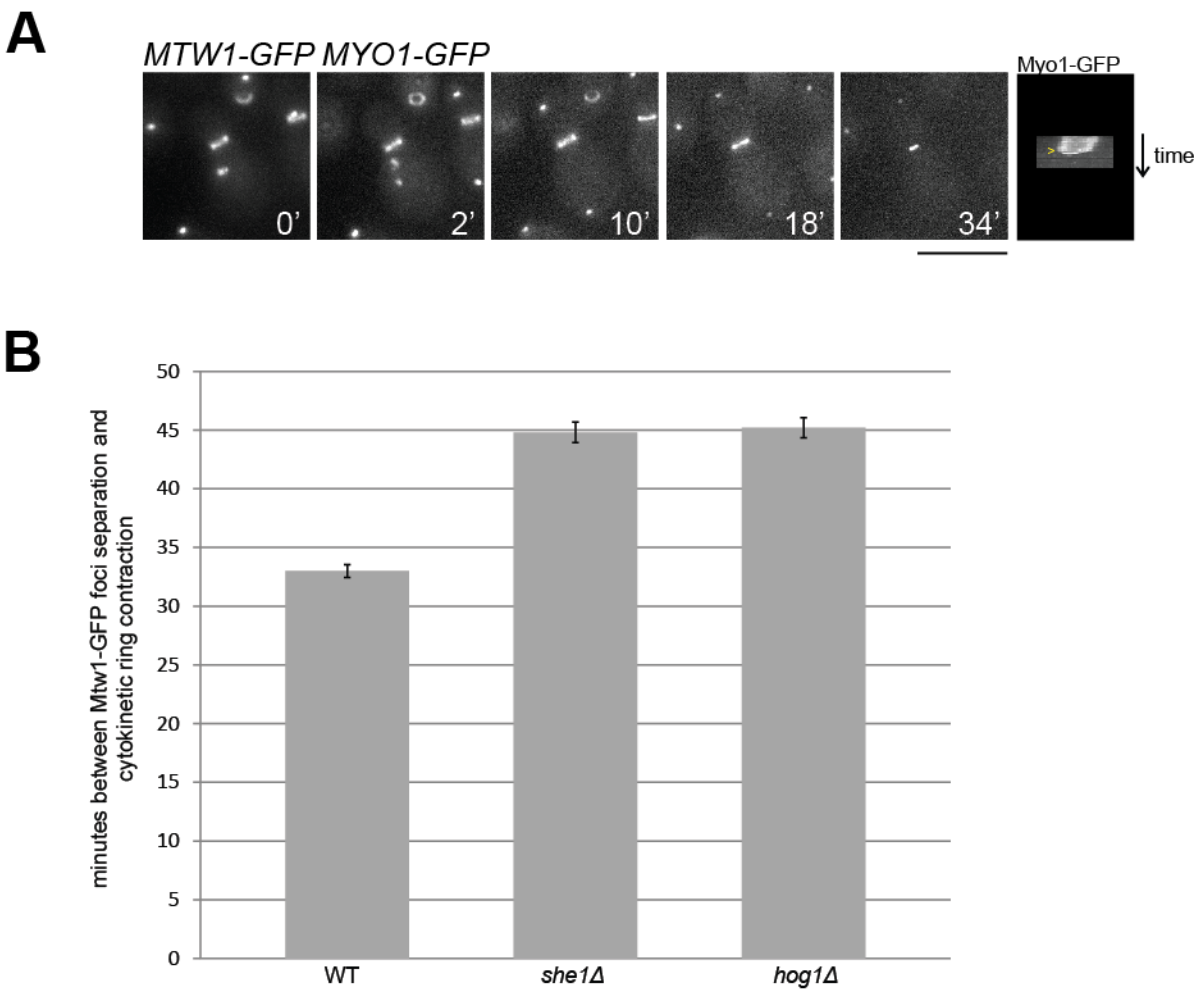

Figure S1 ***she1Δ*** **and** ***hog1Δ*** **mutants have extended M-phases.** (A) Mtw1-GFP Myo1-GFP expressing cells were imaged using time-lapse microscopy, from the time Mtw1-GFP spots separated into two foci until the cytokinetic ring contracted. Right panel: kymograph of Myo1-GFP fluorescence used to determine when the cytokinetic ring began to contract. Bar, 5µm. (B) The time between the appearance of two Mtw1-GFP foci, and the initiation of cytokinetic ring contraction was measured for WT, *she1Δ*, and *hog1Δ* cells.

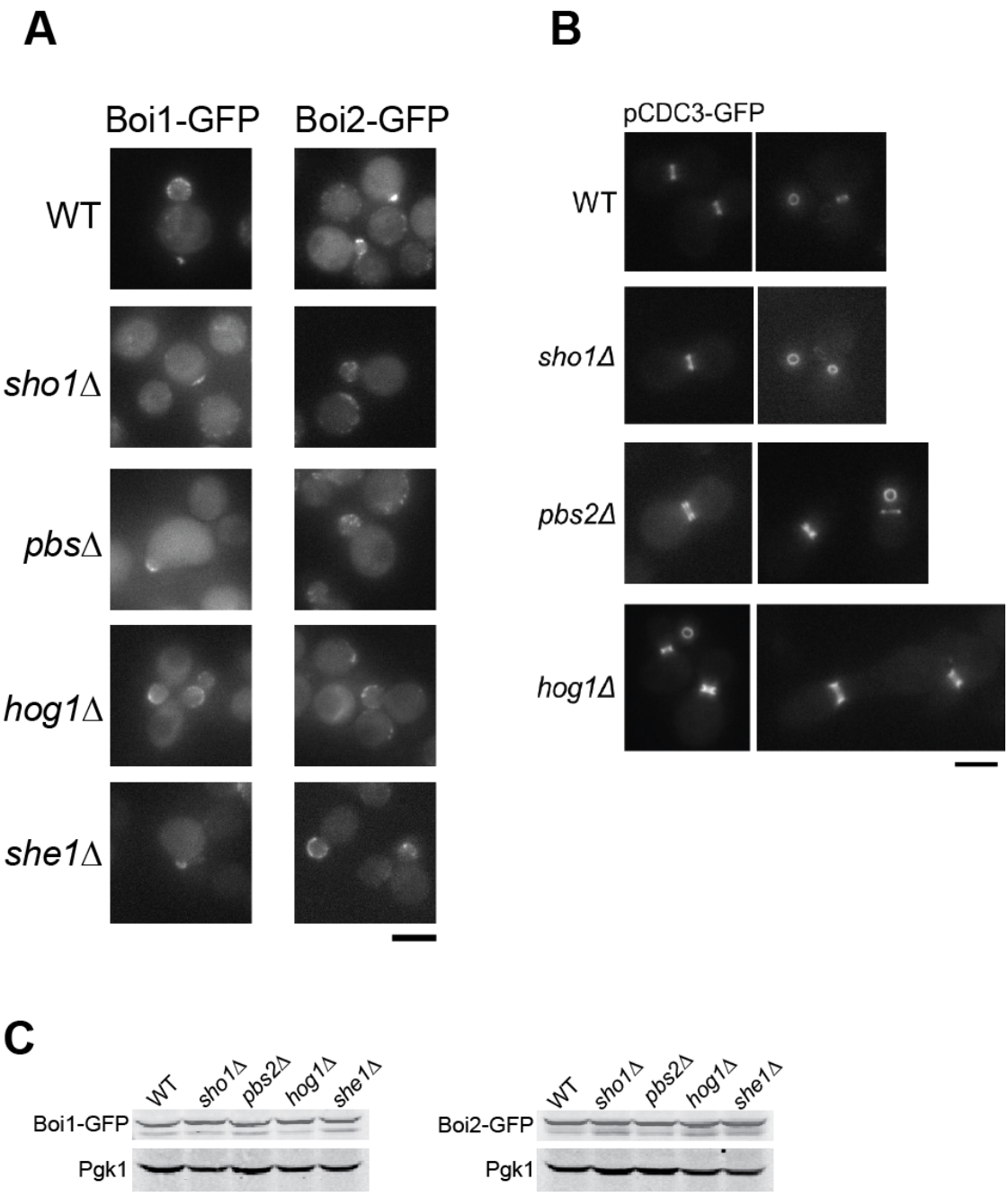

Figure S2 Boi1 and Boi2 localize to the growing bud tip in early mitosis, and the septin Cdc3 is not mislocalized from the bud neck of HOG pathway mutants. (A) Genomically-integrated Boi1-GFP and Boi2-GFP were imaged in living cells of the indicated genotype. Bar, 5µm. Strains of the indicated genotypes were transformed with plasmid-borne *CDC3-GFP* and were imaged using epifluorescence microscopy. Left and right panels were imaged under the same conditions, but show the bud neck from different angles (side-on or end-on). Bar, 5µm. (C) Extracts from Boi1-GFP or Boi2-GFP expressing cells of the indicated genotype were analyzed by western blot using anti-GFP antibodies, and anti-Pgk1 antibodies as a loading control.

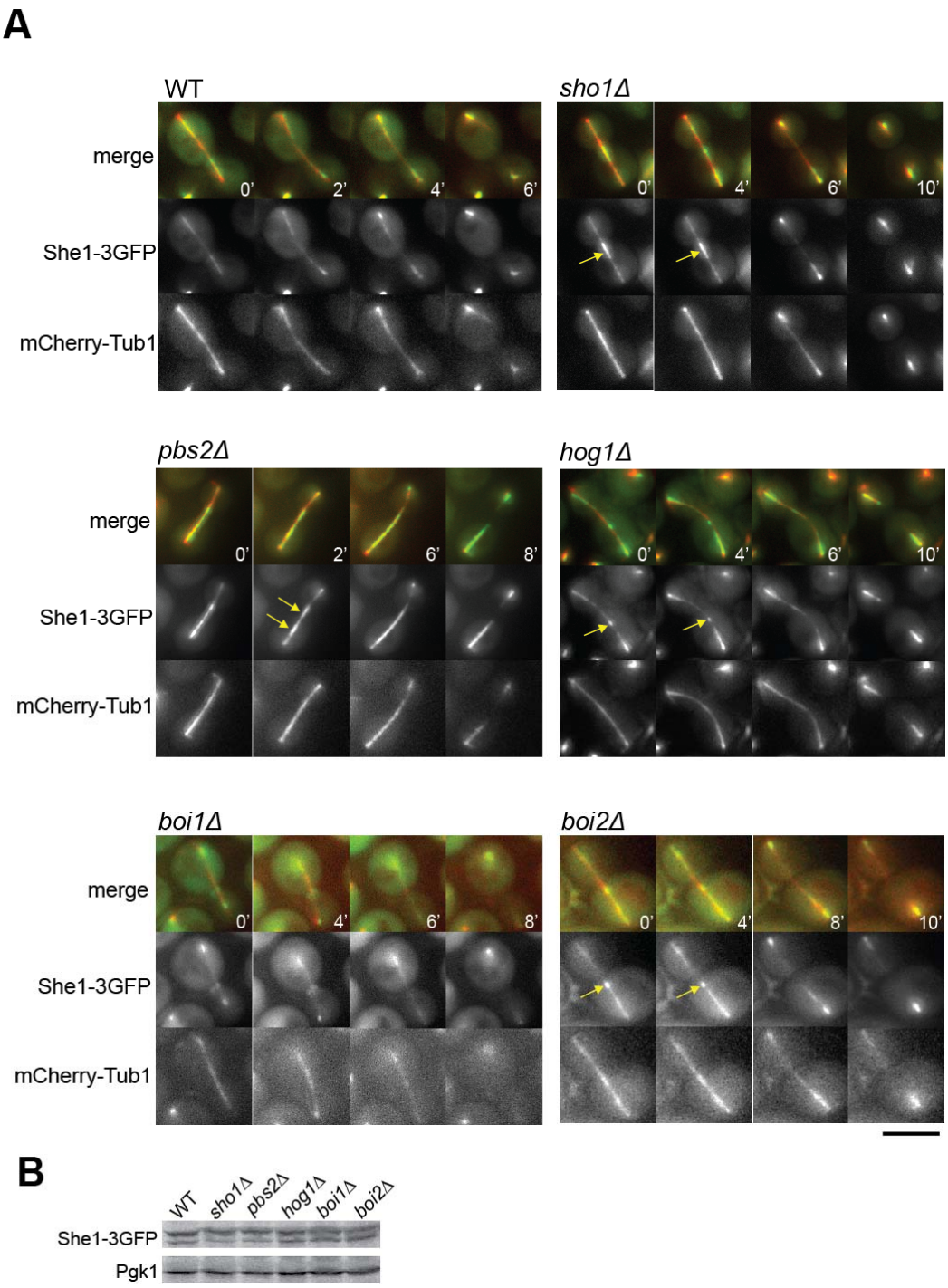

Figure S3 She1-3GFP is mislocalized along the spindle in HOG pathway mutants and *boi2Δ* cells. (A) She1-3GFP mcherry-Tub1 cells of the indicated genotype were imaged using live-cell microscopy. Yellow arrows indicate She1-3GFP that mislocalizes along the spindle. Bar, 5μm. (B) Extracts from She1-3GFP expressing cells of the indicated genotype were analyzed by western blot using anti-GFP antibodies, and anti-Pgk1 antibodies as a loading control.

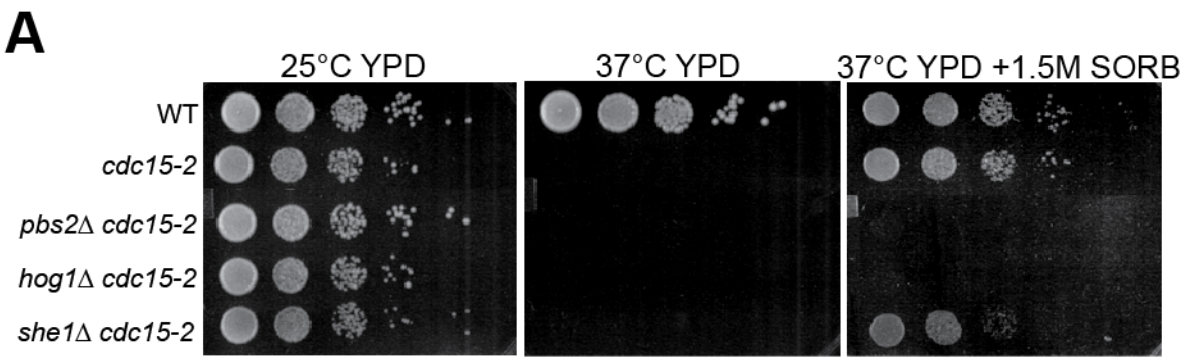
A
25°C YPD
37°C YPD
37°C YPD +1.5M SORB
WT
cdc15-2
pbs2Δ cdc15-2
hog1Δ cdc15-2
she1Δ cdc15-2

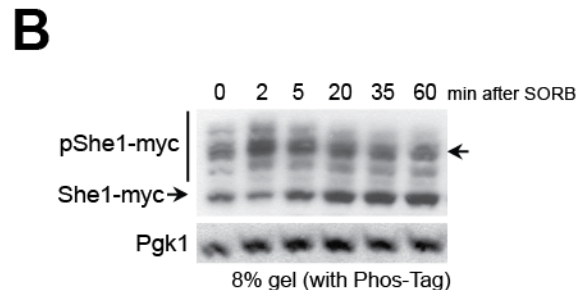
B
0 2 5 20 35 60 min after SORB
pShe1-myc
She1-myc
Pgk1
8% gel (with Phos-Tag)

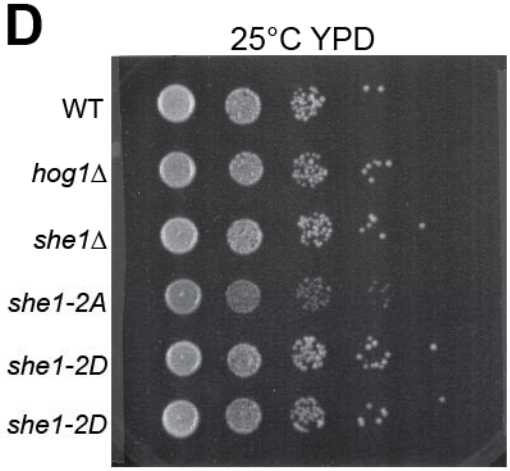
D
25°C YPD
WT
hog1Δ
she1Δ
she1-2A
she1-2D
hog1Δ she1-2D

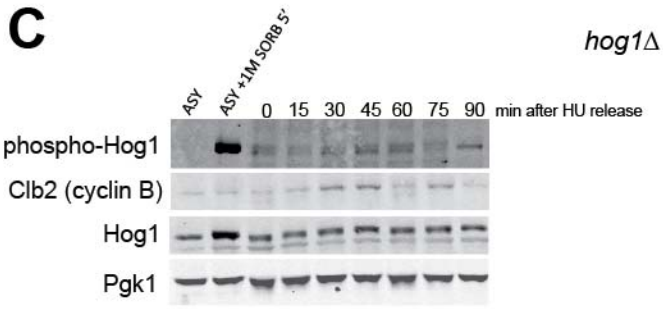
C
ASY
ASY +1M SORB 5'
0 15 30 45 60 75 90 min after HU release
phospho-Hog1
Clb2 (cyclin B)
Hog1
Pgk1

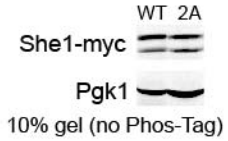
E
WT 2A
She1-myc
Pgk1
10% gel (no Phos-Tag)

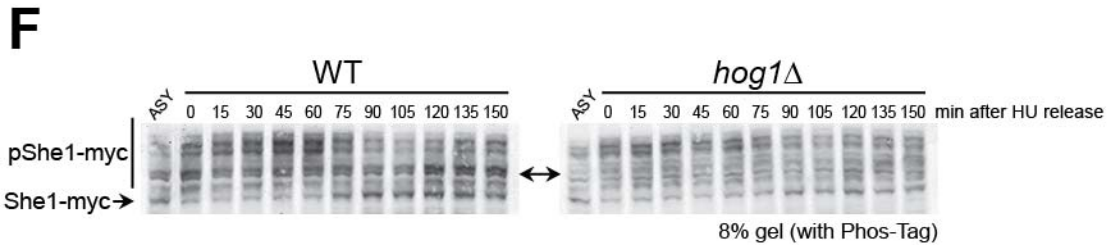
F
WT
hog1Δ
ASY
0 15 30 45 60 75 90 105 120 135 150 min after HU release
pShe1-myc
She1-myc
8% gel (with Phos-Tag)

Figure S4 She1 is required for sorbitol rescue of cdc15-2 cells, is phosphorylated in response to sorbitol stress, and is phosphorylated in part by Hog1. (A) Serial dilutions of cells of the indicated genotype were spotted onto YPD plates, or YPD plates containing 1.5M sorbitol (SORB). (B) She1 is rapidly phosphorylated in response to sorbitol treatment. She1-myc expressing cells were treated with 1M sorbitol, cells were harvested at indicated timepoints, TCA precipitated, and immunoblots of Phos-Tag gels were probed with anti-myc and Pgk1 antibodies. Arrow at right indicates the phospho-species of She1 that is enriched after sorbitol treatment, especially at the 2min timepoint. (C) Hog1 is phosphorylated in a cell-cycle dependent manner. Immunoblots of TCA-precipitated whole cell extracts from Hog1-GFP expressing cells were probed with antibodies against phosphorylated Hog1, GFP (total Hog1), and Clb2. Cells were collected every 15 minutes after hydroxyurea (HU) arrest and washout. ASY: asynchronously growing cultures that were not stressed, or stressed for 5 minutes with 1M Sorbitol to induce Hog1 phosphorylation. (D) Serial dilutions of cells of the indicated genotype were spotted onto YPD plates. (E) She1-myc is expressed at approximately equal levels in *SHE1* and *she1-2A* cells. TCA-precipitated extracts were run on an SDS-PAGE gel without Phos-Tag, and immunblotted with anti-myc and Pgk1 antibodies. (F) She1-myc expressing cells of a WT or *hog1Δ* background were arrested in S-phase with hydroxyurea (HU), and harvested every 15min after HU washout. TCA-precipitated extracts were run on Phos-Tag gels, and immunoblotted with anti-myc antibodies. Shown are two different immunoblots, from gels that were run at the same time in the same gel-box, and processed alongside each other. The immunoblot images are aligned here according to molecular weight markers, so the band size is comparable between the blots. The double-headed arrow between the blots points to a phospho-She1 species that is enriched in WT cells, but not in the *hog1Δ* mutant.

Table S1 Yeast strains used in this study

strain name	mating type	genotype	source
DDY904	*MATα*	*his3Δ200 lys2-801 ura3-52 leu2-3,112* (wild-type)	Drubin/Barnes Lab
DDY4445	*MATa*	*GFP-TUB1::URA3*	Woodruff et al., 2009
DDY4446	*MATa*	*GFP-TUB1::URA3 she1Δ::LEU2*	Woodruff et al., 2009
DDY4447	*MATa*	*MYO1-GFP::HIS3 GFP-TUB1::URA3*	Woodruff et al., 2010
DDY4213	*MATa*	*MYO1-GFP::HIS3 GFP-TUB1::URA3 she1Δ::LEU2*	Woodruff et al., 2010
DDY4407	*MATα*	*sho1Δ::KanMX MYO1-GFP::HIS3 GFP-TUB1::URA3*	this study
DDY4408	*MATα*	*pbs2Δ::LEU2 MYO1-GFP::HIS3 GFP-TUB1::URA3*	this study
DDY4409	*MATα*	*hog1Δ::KanMX MYO1-GFP::HIS3 GFP-TUB1::URA3*	this study
DDY4410	*MATα*	*boi1Δ::LEU2 MYO1-GFP::HIS3 GFP-TUB1::URA3*	this study
DDY4411	*MATα*	*boi2Δ::HIS3 MYO1-GFP::HIS3 GFP-TUB1::URA3*	this study
DDY4412	*MATα*	*sho1Δ::KanMX GFP-TUB1::URA3*	this study
DDY4413	*MATα*	*pbs2Δ::LEU2 GFP-TUB1::URA3*	this study
DDY4414	*MATα*	*hog1Δ::KanMX GFP-TUB1::URA3*	this study
DDY4415	*MATα*	*boi1Δ::LEU2 GFP-TUB1::URA3*	this study
DDY4416	*MATα*	*boi2Δ::HIS3 GFP-TUB1::URA3*	this study
DDY4417	*MATa*	*BOI1-GFP::TRP1*	Jeff Woodruff
DDY4418	*MATa*	*BOI2-GFP::KanMX*	Anthony Cormier, Drubin/Barnes Lab
DDY4419	*MATα*	*sho1Δ::KanMX BOI1-GFP::TRP1*	this study
DDY4420	*MATa*	*pbs2Δ::LEU2 BOI1-GFP::TRP1*	this study
DDY4421	*MATα*	*hog1Δ::KanMX BOI1-GFP::TRP1*	this study
DDY4422	*MATα*	*she1Δ::LEU2 BOI1-GFP::TRP1*	Jeff Woodruff, Drubin/Barnes Lab
DDY4423	*MATα*	*sho1Δ::KanMX BOI2-GFP::KanMX*	this study
DDY4424	*MATα*	*pbs2Δ::LEU2 BOI2-GFP::KanMX*	this study
DDY4425	*MATα*	*hog1Δ::KanMX BOI2-GFP::KanMX*	this study
DDY4426	*MATα*	*she1Δ::LEU2 BOI2-GFP::KanMX*	this study
DDY4448	*MATa*	*SHE1-3GFP::HIS3*	Woodruff et al., 2009
DDY4427	*MATa*	*sho1Δ::KanMX SHE1-3GFP::HIS3*	this study
DDY4428	*MATa*	*pbs2Δ::LEU2 SHE1-3GFP::HIS3*	this study
DDY4429	*MATa*	*hog1Δ::KanMX SHE1-3GFP::HIS3*	this study
DDY4430	*MATa*	*boi1Δ::LEU2 SHE1-3GFP::HIS3*	this study
DDY4431	*MATa*	*boi2Δ::HIS3 SHE1-3GFP::HIS3*	this study
DDY4432	*MATα*	*HOG1-GFP::KanMX*	this study
DDY4449	*MATa*	*SHE1-13MYC::HIS3*	Woodruff et al., 2010

Table S1 Yeast strains used in this study (continued)

strain name	mating type	genotype	source
DDY4433	*MATa*	*she1-2A-13MYC::HIS3::URA3::she1Δ::LEU2*	this study
DDY4434	*MATa*	*hog1-as::hphNT1 MYO1-GFP::HIS3 GFP-TUB1::URA3*	this study
DDY4435	*MATa*	*she1-2A::URA3::she1Δ::LEU2 MYO1-GFP::HIS3 GFP-TUB1::URA3*	this study
DDY4436	*MATa*	*hog1-as::hphNT1 SHE1-3GFP::HIS*	this study
DDY4437	*MATa*	*cdc15-2 CDC14-GFP::KanMX mCherry-TUB1::URA3*	this study
DDY4438	*MATa*	*cdc15-2 hog1Δ::KanMX CDC14-GFP::KanMX mCherry-TUB1::URA3*	this study
DDY4439	*MATa*	*cdc15-2 pbs2Δ::LEU2 CDC14-GFP::KanMX mCherry-TUB1::URA3*	this study
DDY4440	*MATa*	*cdc15-2 she1Δ::LEU2 CDC14-GFP::KanMX mCherry-TUB1::URA3*	this study
DDY4441	*MATα*	*pCDC3-GFP::URA3* in DDY 904	this study
DDY4442	*MATα*	*pCDC3-GFP::URA3* in *sho1Δ::KanMX*	this study
DDY4443	*MATa*	*pCDC3-GFP::URA3* in *hog1Δ::KanMX*	this study
DDY4444	*MATa*	*pCDC3-GFP::URA3* in *pbs2Δ::LEU2*	this study
DDY4691	*MATa*	*she1Δ::LEU2 hog1Δ::KanMX MYO1-GFP::HIS3 GFP-TUB1::URA3*	this study
DDY4692	*MATa*	*kip3Δ::KanMX hog1Δ::KanMX MYO1-GFP::HIS3 GFP-TUB1::URA3*	this study
DDY4693	*MATa*	*cdh1Δ::KanMX hog1Δ::KanMX MYO1-GFP::HIS3 GFP-TUB1::URA3*	this study
DDY4694	*MATa*	*MTW1-GFP::HIS3 MYO1-GFP::HIS3*	this study
DDY4695	*MATα*	*she1Δ::LEU2 MTW1-GFP::HIS3 MYO1-GFP::HIS3*	this study
DDY4696	*MATα*	*hog1Δ::KanMX MTW1-GFP::HIS3 MYO1-GFP::HIS3*	this study
DDY4206	*MATα*	*SHE1-3GFP::HIS3 mCherry-TUB1::URA3*	Woodruff et. al 2010
DDY4697	*MATα*	*sho1Δ::KanMX SHE1-3GFP::HIS3 mCherry-TUB1::URA3*	this study
DDY4698	*MATα*	*pbs2Δ::LEU2 SHE1-3GFP::HIS3 mCherry-TUB1::URA3*	this study
DDY4799	*MATα*	*hog1Δ::KanMX SHE1-3GFP::HIS3 mCherry-TUB1::URA3*	this study
DDY4700	*MATα*	*boi1Δ::LEU2 SHE1-3GFP::HIS3 mCherry-TUB1::URA3*	this study
DDY4701	*MATα*	*boi2Δ::HIS3 SHE1-3GFP::HIS3 mCherry-TUB1::URA3*	this study
DDY4702	*MATa*	*cdc15-2* (backcrossed)	this study
DDY4703	*MATa*	*pbs2Δ::LEU2 cdc15-2*	this study
DDY4704	*MATa*	*hog1Δ::KanMX cdc15-2*	this study
DDY4705	*MATa*	*she1Δ::LEU2 cdc15-2*	this study
DDY4706	*MATa*	*she1-2A::URA3::she1Δ::LEU2*	this study
DDY4707	*MATa*	*she1-2D::URA3::she1Δ::LEU2*	this study
DDY4708	*MATa*	*she1-2D::URA3::she1Δ::LEU2 hog1Δ::KanMX*	this study
DDY4709	*MATα*	*she1-2D::URA3::she1Δ::LEU2 hog1Δ::KanMX MYO1-GFP::HIS3 GFP-TUB1::URA3*	this study
DDY4710	*MATa*	*she1-2D::URA3::she1Δ::LEU2 hog1-as::hphNT1 MYO1-GFP::HIS3 GFP-TUB1::URA3*	this study

Table S1 Yeast strains used in this study (continued)

strain name	mating type	genotype	source
DDY4711	*MATa*	*hog1Δ::KanMX SHE1-13MYC::HIS3*	this study
DDY4712	*MATa*	*she1-2A::URA3::she1Δ::LEU2 GFP-TUB1::URA3*	this study
DDY4713	*MATa*	*hog1-as::hphNT1 GFP-TUB1::URA3*	this study
DDY4714	*MATα*	*she1-2D::URA3::she1Δ::LEU2 hog1Δ::KanMX GFP-TUB1::URA3*	this study
DDY4715	*MATa*	*she1-2D::URA3::she1Δ::LEU2 hog1-as::hphNT1 GFP-TUB1::URA3*	this study

References:

Woodruff, J. B., D. G. Drubin, and G. Barnes, 2009 Dynein-driven mitotic spindle positioning restricted to anaphase by She1p inhibition of dynactin recruitment. Mol. Biol. Cell. 20: 3003-3011.

Woodruff, J. B., D. G. Drubin, and G. Barnes, 2010 Mitotic spindle disassembly occurs via distinct subprocesses driven by the anaphase-promoting complex, Aurora B kinase, and kinesin-8. J. Cell Biol. 191: 795-808.